# 10 Adaptive Space-Time Processing for Wireless CDMA

Sofiène Affes and Paul Mermelstein

INRS-Telecommunications, University of Quebec
800, de la Gauchetière Ouest, Suite 6900
Montreal, Quebec, H5A 1K6, Canada
E-mail: {affes, mermel}@inrs-telecom.uquebec.ca

**Abstract.** We consider adaptive space-time processing for wireless receivers in CDMA networks. Currently, the 2D RAKE is the most widely used space-time array-processor which combines multipath signals sequentially, first in space, then in time. We introduce incremental processing improvements to arrive ultimately at a more efficient one-dimensional joint space-time (1D-ST) adaptive processor named STAR, the spatio-temporal array-receiver. STAR improves the receiver's performance by approaching blind coherent space-time maximum ratio combining (ST-MRC). With blind quasi-coherent joint ST-MRC, STAR outperforms the 2D RAKE by improving the combing operation with 2 dB gain in SNR. With quasi-blind coherent joint ST-MRC, STAR can enhance channel identification while reducing significantly the pilot-power or -overhead fraction leading to a 1 dB gain in SNR. These gains translate to significant performance advantage for all versions of 1D-ST STAR over current 2D RAKE-type receivers.

## 10.1 Introduction

Recently adopted standards confirm that CDMA is the preferred air-interface technology for third-generation wireless systems [1]-[3]. They also recognize adaptive antenna arrays as key means to increasing capacity and spectrum efficiency. In the context of this important real-world application, adaptive space-time processing can respond to the need for fast and reliable transmission over the noisy and time-varying channels encountered in wireless access. Adaptive space-time processing addresses a broad range of issues that aim to improve: 1) multipath channel identification and combining [4], 2) synchronization [4], [5], 3) interference reduction [6] or suppression [7], etc... We focus here on the first issue and propose useful upgrades of the 2D RAKE [8]-[11] that ultimately implement a more efficient adaptive array-processor, STAR, the spatio-temporal array-receiver [4], [5].

The 2D RAKE, developed first by a research group at Stanford University [8]-[11], is a two-dimensional space-time adaptive array-processor widely investigated today which combines signals sequentially, first in space, then in time over CDMA multipath Rayleigh-fading channels. In the blind mode (*i.e.*, without a pilot), the 2D-RAKE receivers estimate the channel with phase ambiguities and implement sequential combining, first noncoherent

J. Benesty et al. (eds.), *Adaptive Signal Processing*
© Springer-Verlag Berlin Heidelberg 2003

spatial MRC, followed by temporal equal-gain combining (EGC). In the pilot-assisted mode they use the pilot for channel identification [12]-[16] and hence require a pilot with sufficient power to estimate the channel accurately and implement first reference-assisted coherent spatial MRC followed by temporal MRC. This contribution considers an adaptive array-receiver that significantly improves receiver performance and approaches that of blind coherent joint ST-MRC.

First, in the blind mode we exploit the flexibility of the decision-feedback identification (DFI) procedure [4], [17] for channel estimation in the STAR receiver [4], [5] to arrive at a 2D-RAKE with an initial feedback mode in an improved adaptive structure. Further upgrades of the feedback mode in the DFI procedure ultimately enable identification of the channel within a constellation-invariant phase ambiguity and hence allow implementation of quasi-coherent (*i.e.*, differential decoding after coherent detection) joint ST-MRC with about 2 dB gain in SNR.

Second, in the pilot-assisted mode we exploit a much weaker pilot than needed by the 2D-RAKE receiver to estimate then compensate the constellation-invariant phase ambiguity of the channel identified blindly and more accurately and therefore implement quasi-blind or asymptotically blind coherent joint ST-MRC [18], [19], [21]. Thereby STAR can outperform the 2D-RAKE receiver by enhancing channel identification and by significantly reducing the pilot power or overhead fraction (in the range of 1%) and the resulting interference. Both enhancements combined result in a total SNR gain of 1 dB and enable significant battery power-savings and spectrum-efficiency gains.

This upgrade process allows us to replace the sequential spatial-temporal processing in 2D RAKE-type receivers by one-dimensional joint space-time (1D-ST) processing in STAR and thereby improve channel identification. We present novel and significant analytical results [17], [19] that establish clearly the performance advantages of one-dimensional joint space-time processing in 1D-ST STAR over two-dimensional spatial then temporal sequential processing widely implemented today in 2D RAKE-type receivers. We show that 1D-ST structured adaptive receivers reduce both complexity and channel identification errors, increase robustness to changing propagation conditions, and speed up convergence over multipath Rayleigh-fading channels.

Organization of this chapter is as follows: in Sect. 10.2 we describe our data model then provide a brief overview of the blind 2D RAKE receiver in Sect. 10.3. Section 10.4 proposes incremental upgrades of the 2D RAKE that ultimately implement blind quasi-coherent ST-MRC in 2D STAR. In Sect. 10.5, we show the benefits of joint space-time processing in the blind 1D-ST STAR. Section 10.6 considers a last option, namely the use of very weak pilot signals for channel ambiguity estimation and resolution which implement quasi-blind coherent joint ST-MRC. We finally draw our conclusions

in Sect. 10.7. Simulations of the enhancements at each stage validate the significant performance gains achievable with the 1D-ST STAR receiver.

## 10.2 Data Model

We consider uplink transmission with $M$ receiving antennas at the base-station. Extension to the downlink with multi-antenna mobile stations follows along similar lines but the details are left for future consideration. We consider a multipath Rayleigh fading environment with number of paths $P$ and Doppler spread frequency $f_D$. For simplicity, we assume perfect synchronization of the multipath delays. Efficient incorporation of accurate timing in CDMA receivers is addressed in [4], [5].

For air-interface transmission[1] we use $\mathcal{M}$PSK modulation, defined by the following constellation set of $\mathcal{M}$ symbols:

$$\mathcal{C}_{\mathcal{M}} = \{\ldots, c_k, \ldots\} = \left\{\ldots, e^{j\frac{(2k-1-\delta(\mathcal{M}-2))}{\mathcal{M}}\pi}, \ldots\right\},\ k \in \{1, \ldots, \mathcal{M}\}, \quad (10.1)$$

where $\delta(x) = 1$ if $x = 0$, and 0 otherwise. The data symbols $\underline{b}_n \in \mathcal{C}_{\mathcal{M}}$ are $\mathcal{M}$PSK-modulated at the rate $1/T_s$ where $T_s$ is the symbol duration then differentially encoded as:

$$b_n = \underline{b}_n b_{n-1} e^{-j(1-\delta(\mathcal{M}-2))\pi/\mathcal{M}}, \quad (10.2)$$

and hence ideally differentially decoded as:

$$\underline{b}_n = b_n b_{n-1}^* e^{j(1-\delta(\mathcal{M}-2))\pi/\mathcal{M}}. \quad (10.3)$$

The phase offset $e^{-j(1-\delta(\mathcal{M}-2))\pi/\mathcal{M}}$ keeps both $b_n$ and $\underline{b}_n$ in the $\mathcal{M}$PSK constellation set $\mathcal{C}_{\mathcal{M}}$ in the differential encoding and decoding steps, respectively. We also define the set of constellation-invariant phase rotations as:

$$\mathcal{R}_{\mathcal{M}} = \{\ldots, r_k, \ldots\} \text{ s.t. } \forall\ k' \in \{1, \ldots, \mathcal{M}\}\ r_k c_{k'} \in \mathcal{C}_{\mathcal{M}}, \quad (10.4)$$

referred to in the following as the *rotation set*. For $\mathcal{M}$PSK modulations, the rotation set is given by[2]:

$$\mathcal{R}_{\mathcal{M}} = \left\{\ldots, e^{j2(k-1)\pi/\mathcal{M}}, \ldots\right\},\ k \in \{1, \ldots, \mathcal{M}\}. \quad (10.5)$$

After despreading the data at the receiver, we form the $M \times 1$ multipath despread vector for each path $p = 1, \ldots, P$:

$$Z_{p,n} = G_{p,n}\varepsilon_{p,n}\psi_n b_n + N_{p,n} = G_{p,n}\zeta_{p,n} b_n + N_{p,n} = G_{p,n} s_{p,n} + N_{p,n}, \quad (10.6)$$

[1] The HSDPA standard [3] suggests use of high-order modulations such as $\mathcal{M}$PSK and $\mathcal{M}$QAM (see Sects. 10.4.5 and 10.6.6) in order to increase the peak rate.

[2] Note that the $\mathcal{M}$PSK constellation set $\mathcal{C}_{\mathcal{M}}$ can be equated to its rotation set $\mathcal{R}_{\mathcal{M}}$, thereby allowing suppression of the phase offset $e^{-j(1-\delta(\mathcal{M}-2))\pi/\mathcal{M}}$ in both (10.2) and (10.3). For the sake of generalization, however, we use the conventional $\mathcal{M}$PSK constellations of (10.1) where $\mathcal{C}_{\mathcal{M}} \neq \mathcal{R}_{\mathcal{M}}$.

**Table 10.1** Parameters used in the illustrations.

| Parameter | Value | Comment |
|---|---|---|
| $1/T_s$ | 19.2 KBaud | Baud rate |
| $M$ | 4 | number of antennas |
| $P$ | 3 | number of fading paths |
| $\bar{\varepsilon}_p^2$ | (0, 0, 0) dB | average power profile |
| $f_c$ | 1.9 GHz | carrier frequency |
| $f_D$ | 9 Hz | Doppler spread (*i.e.*, 5 Kmph) |
| $f_{PC}$ | 1600 Hz | power control (PC) frequency |
| $\Delta P_{PC}$ | $\pm$ 0.25 dB | PC adjustment |
| $BER_{PC}$ | 10 % | PC-command BER |
| $\tau_{PC}$ | 0.625 ms | PC transmission delay |
| $\mu$ | 0.05 | adaptation step-size |
| $SNR_{\text{in}}$ | $2 - 10\log_{10}\left[\sin(\pi/\mathcal{M})^2\right]$ | SNR after despreading in dB |

where $s_{p,n} = \varepsilon_{p,n}\psi_n b_n = \zeta_{p,n} b_n$ is the multipath signal component, $\psi_n^2$ is the total received power and $\varepsilon_{p,n}^2$ is the normalized power fraction (*i.e.*, $\sum_{p=1}^{P} \varepsilon_{p,n}^2 = 1$) of the total power received over the $p$-th path $\zeta_{p,n}^2 = \varepsilon_{p,n}^2 \psi_n^2$. The $M \times 1$ vector $G_{p,n}$, with norm[3] $\sqrt{M}$, denotes the channel vector from the transmitter to the multi-antenna receiver over the $p$-th multipath. The interference vectors $N_{p,n}$, mutually independent, have identical spatially-uncorrelated Gaussian distribution with mean zero and covariance matrix $\mathbf{R}_N = \sigma_N^2 \mathbf{I}_M$ after despreading of the data channel. The resulting input SNR after despreading is $SNR_{\text{in}} = \bar{\psi}^2/\sigma_N^2$ per antenna element where $\bar{\psi}^2$ denotes the average total received power. Uncorrelated-Gaussian assumption holds when a large number of users are active. This motivates us to implement coherent maximum ratio combining (MRC) in both space and time, the optimal combiner in this case. Otherwise, for colored noise situations, we may incorporate the optimum or the multi-user combining solutions proposed in [6] and [7], respectively; but that is beyond the scope of this contribution.

The performance of the various receiver structures is verified by simulations at the physical level with parameters[4] listed in Table 10.1. Enhancements in terms of capacity at specified transmission rates are best estimated by system-level simulations [18], [19], but those are beyond the scope of this contribution.

[3] The normalization factors of $\|G_{p,n}\|^2$ (in space) and $\varepsilon_{p,n}^2$ (in time) are both included in $\psi_n^2$.

[4] The last two parameters of Table 10.1 are only used in Figs. 10.1 to 10.8. The SNR value guarantees the same nominal SER for all modulations (see also SNR in Fig. 10.8 for 16QAM).

## 10.3 The Blind 2D RAKE Receiver

To the best of our knowledge, the blind 2D RAKE was the first adaptive array-processing receiver-structure proposed for DBPSK-modulated CDMA signals [8]-[11]. This receiver is adaptive in that it carries out iterative channel identification in order to implement noncoherent spatial MRC. The blind channel identification step of the 2D RAKE will be explained shortly below. Here, we extend the 2D-RAKE to D$\mathcal{M}$PSK-modulated CDMA signals.

For now, assume that estimates of the propagation vectors with phase ambiguities are available at each iteration $n$ (*i.e.*, $\hat{G}_{p,n} \simeq e^{-j\phi_{p,n}} G_{p,n}$). The 2D RAKE first estimates the multipath signal component $\tilde{s}_{p,n}$ over each path for $p = 1, \ldots, P$ by noncoherent spatial MRC:

$$\tilde{s}_{p,n} = \frac{\hat{G}_{p,n}^H Z_{p,n}}{M} \simeq e^{j\phi_{p,n}} \psi_n \varepsilon_{p,n} b_n + \frac{\hat{G}_{p,n}^H N_{p,n}}{M} \simeq e^{j\phi_{p,n}} s_{p,n} + \eta_{p,n}, \quad (10.7)$$

where the residual interference $\eta_{p,n}$ is zero-mean complex Gaussian with variance $\sigma_N^2/M$. The 2D RAKE thereby implements the so called "antenna gain" by reducing the level of interference by a factor $M$ at the combiner output. Second, to alleviate the impact of the phase ambiguities $\phi_{p,n}$, the 2D RAKE resorts to noncoherent temporal differential demodulation and EGC of the multipath signal component estimates in the following decision variable:

$$d_n = \sum_{p=1}^{P} \tilde{s}_{p,n} \tilde{s}_{p,n-1}^*, \quad (10.8)$$

and hence estimates the $\mathcal{M}$PSK symbol $\underline{b}_n$ from $d_n$ as follows:

$$\hat{\underline{b}}_n = \arg\min_{c_k \in \mathcal{C}_\mathcal{M}} \left\{ \left| d_n e^{j(1-\delta(\mathcal{M}-2))\pi/\mathcal{M}} - c_k \right| \right\}. \quad (10.9)$$

In a channel-coded transmission, the 2D RAKE passes on $d_n$ directly to the channel decoder after appropriate mapping. For power control, the total received power can be estimated by simple smoothing as follows:

$$\hat{\psi}_{n+1}^2 = (1-\alpha)\hat{\psi}_n^2 + \alpha \left( \sum_{p=1}^{P} |\tilde{s}_{p,n}|^2 \right), \quad (10.10)$$

where $\alpha \ll 1$ is a smoothing factor. An equivalent estimator of the total received power sums up estimates of the received powers over paths $\hat{\zeta}_{p,n}^2 = \hat{\varepsilon}_{p,n}^2 \hat{\psi}_n^2$ and allows estimation of the normalized power fractions $\hat{\varepsilon}_{p,n}^2$ as follows:

$$\hat{\zeta}_{p,n+1}^2 = (1-\alpha)\hat{\zeta}_{p,n}^2 + \alpha |\tilde{s}_{p,n}|^2, \quad (10.11)$$

$$\hat{\psi}_{n+1}^2 = \sum_{p=1}^{P} \hat{\zeta}_{p,n+1}^2, \quad (10.12)$$

$$\hat{\varepsilon}_{p,n+1}^2 = \hat{\zeta}_{p,n+1}^2 / \left( \sum_{p=1}^{P} \hat{\zeta}_{p,n+1}^2 \right) = \hat{\zeta}_{p,n+1}^2 / \hat{\psi}_{n+1}^2. \quad (10.13)$$

The normalized power fraction estimates $\hat{\varepsilon}_{p,n}^2$ are of no immediate use in the blind 2D RAKE. However, they will be exploited later to significantly enhance 2D space-time receivers.

As mentioned above, estimates of propagation vectors $\hat{G}_{p,n}$ are required to implement noncoherent spatial MRC of (10.7) in the 2D RAKE. Exploiting the fact that the interference vector in (10.6) is an uncorrelated white noise vector, the propagation vector over each path $G_{p,n}$ can be identified as the principal eigenvector of $\mathbf{R}_{Z_p}$, the correlation matrix of the despread vector $Z_{p,n}$ over the $p$-th path:

$$\begin{aligned}\mathbf{R}_{Z_p} &= E\left[Z_{p,n}Z_{p,n}^H\right] = \bar{\psi}^2\bar{\varepsilon}_p^2 G_p G_p^H + \sigma_N^2\mathbf{I}_M \\ &= \bar{\psi}^2\bar{\varepsilon}_p^2\left(e^{-j\phi_p}G_p\right)\left(e^{-j\phi_p}G_p\right)^H + \sigma_N^2\mathbf{I}_M,\end{aligned} \tag{10.14}$$

where $\bar{\psi}^2$ and $\bar{\varepsilon}_p^2$ are the average total received power and the multipath power fraction, respectively. In practice, each vector $G_{p,n}$ is estimated within an unknown phase ambiguity $\phi_{p,n}$ by an iterative principal component analysis (PCA) method based on a singular- or eigenvalue decomposition of the sample correlation matrix $\hat{\mathbf{R}}_{Z_p}$ [8]-[11]. However, in the next section we show that this iterative PCA method can be replaced by an adaptive channel identification technique that is less complex and performs better.

In summary, the blind 2D RAKE [8]-[11] implements noncoherent spatial MRC and achieves an antenna gain by reducing the interference power by a factor equal to the number of antennas and thereby improves capacity significantly. Additional enhancements may be introduced until the noncoherent differential temporal demodulation and EGC step of (10.9) is completely replaced by quasi-coherent (*i.e.*, within a constellation-invariant phase ambiguity rotation) MRC in both space and time, without a pilot.

## 10.4 The Blind 2D STAR

We propose incremental upgrades of the blind 2D RAKE that ultimately lead to a very efficient blind quasi-coherent (*i.e.*, within a constellation-invariant phase rotation) ST-MRC combiner. The resulting improvement in the combining operation offers about 2 dB gain in SNR with all tested $\mathcal{M}$PSK modulations.

### 10.4.1 Decision-Feedback Identification (DFI)

We introduce an adaptive channel identification procedure that offers a unifying framework in terms of a common structure called the spatio-temporal array-receiver (STAR) [4], [5] by equipping various combiners of D$\mathcal{M}$PSK-modulated signals with the same channel identification engine. Starting with the conventional 2D-RAKE, we consider successive simple modifications to

the feedback signal and obtain incremental improvements until we reach a blind quasi-coherent ST-MRC combiner.

This procedure, referred to as decision-feedback identification (DFI) [4], [17], updates the channel estimate[5] as follows:

$$\hat{G}_{p,n+1} = \hat{G}_{p,n} + \mu_p \left( Z_{p,n} - \hat{G}_{p,n} \hat{s}_{p,n} \right) \hat{s}^*_{p,n}, \tag{10.15}$$

where $\mu_p$ is an adaptation step-size, and $\hat{s}_{p,n}$ is a feedback signal providing a selected estimate of the signal component. We show next how improved choices of the feedback signal lead to enhanced versions of the 2D STAR receiver.

### 10.4.2 Parallel and Soft DFI

In a first version of 2D STAR, we implement *parallel* and *soft* DFI in that 1) the DFI procedures of (10.15) over multipaths for $p = 1, \ldots, P$ are excited with independent feedback signals (*i.e.*, parallel), and 2) the feedback signals are assigned the soft output values of the noncoherent MRC combiners in (10.7) (*i.e.*, soft):

$$\hat{s}_{p,n} = \tilde{s}_{p,n}. \tag{10.16}$$

Substituting $\hat{s}_{p,n}$ for $\tilde{s}_{p,n}$ in (10.7), the DFI procedure of (10.15) can be rewritten as:

$$\begin{aligned} \hat{G}_{p,n+1} &= \hat{G}_{p,n} + \mu_p \left( Z_{p,n} - \hat{G}_{p,n} \hat{G}^H_{p,n} Z_{p,n}/M \right) Z^H_{p,n} \hat{G}_{p,n}/M \\ &= \hat{G}_{p,n} + \mu_p \left( \mathbf{I}_M - \hat{G}_{p,n} \hat{G}^H_{p,n}/M \right) Z_{p,n} Z^H_{p,n} \hat{G}_{p,n}/M \\ &= \hat{G}_{p,n} + \mu_p \mathbf{\Pi}_{p,n} \dot{\mathbf{R}}_{Z_p} \hat{G}_{p,n}/M, \end{aligned} \tag{10.17}$$

and its adaptation gradient now interprets as a projector $\mathbf{\Pi}_{p,n}$ orthogonal to $\hat{G}_{p,n}$ of $\dot{\mathbf{R}}_{Z_p}$, the instantaneous estimate of the correlation matrix $\mathbf{R}_{Z_p}$. On average, adaptation errors are minimized when the projector $\mathbf{\Pi}_{p,n}$ suppresses the dimension of $\mathbf{R}_{Z_p}$ with the highest energy, *i.e.*, its principal eigenvector $e^{-j\phi_{p,n}} G_{p,n}$ [note that $\mathbf{\Pi}_{p,n} \mathbf{R}_{Z_p} G_{p,n} = \mathbf{\Pi}_{p,n} \times (\lambda G_{p,n}) = 0$ if $\hat{G}_{p,n} = \lambda' G_{p,n}$, see (10.14)]. The DFI procedure is therefore an adaptive PCA implementation. Hence, after convergence we have $\hat{G}_{p,n} \simeq e^{-j\phi_{p,n}} G_{p,n}$ and $\hat{s}_{p,n} = \tilde{s}_{p,n} \simeq e^{j\phi_{p,n}} s_{p,n} + \eta_{p,n}$ [see (10.7)].

For illustration purposes, we define the channel ambiguity over each path $a_{p,n}$ and the centroid channel ambiguity $a_n$ as:

$$a_{p,n} = \rho_{p,n} e^{j\phi_{p,n}} = \hat{G}^H_{p,n} G_{p,n}/M \qquad \text{for} \quad p = 1, \ldots, P, \tag{10.18}$$

$$a_n = \rho_n e^{j\phi_n} = \sum_{p=1}^{P} \hat{\varepsilon}_{p,n} \varepsilon_{p,n} \hat{G}^H_{p,n} G_{p,n}/M = \sum_{p=1}^{P} \hat{\varepsilon}_{p,n} \varepsilon_{p,n} a_{p,n}. \tag{10.19}$$

[5] Preferably $\|\hat{G}_{p,n}\|$ is forced to $\sqrt{M}$ after each DFI update for increased stability (we do so in this work), although normalization of $\hat{G}_{p,n}$ to $\sqrt{M}$ is asymptotically guaranteed after convergence.

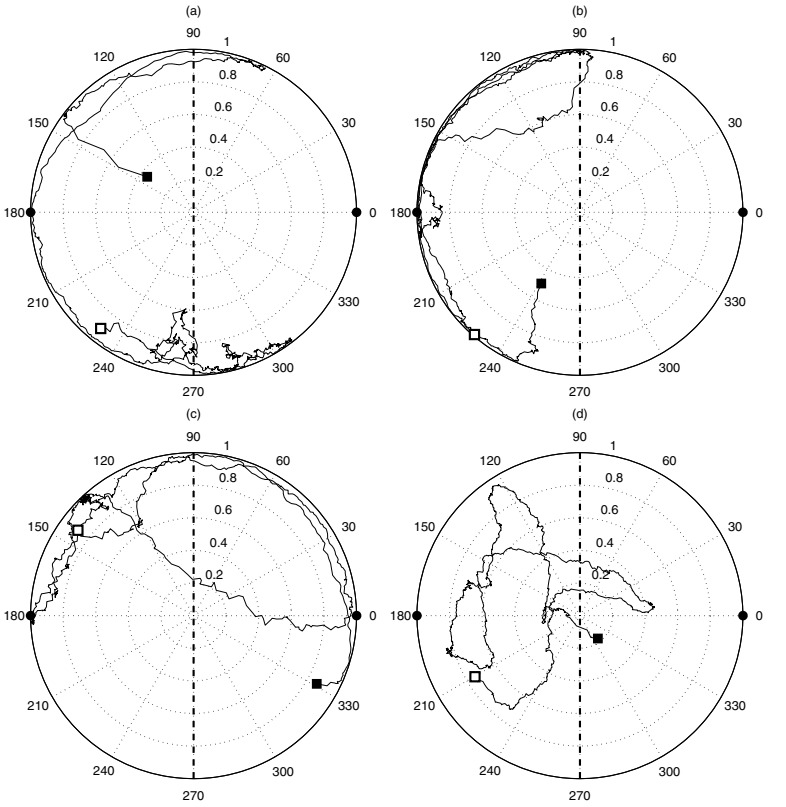


**Fig. 10.1.** Channel ambiguity with BPSK-modulated parallel/soft DFI over (a): 1st path (*i.e.*, $a_{1,n}$), (b): 2nd path (*i.e.*, $a_{2,n}$), (c): 3rd path (*i.e.*, $a_{3,n}$), (d): centroid channel ambiguity (*i.e.*, $a_n$). Constellation-invariant rotation points (*i.e.*, $r_k \in \mathcal{R}_{\mathcal{M}}$) are denoted by black circles and initial/final channel ambiguities by black/white squares.

Figure 10.1 shows that $a_{p,n}$, with parallel/soft DFI, follows the shortest path from initial position $a_{p,0}$ towards the unit circle in the learning phase then remains in its vicinity after convergence (*i.e.*, $\rho_{p,n} = |a_{p,n}| \simeq 1$ and $a_{p,n} \simeq e^{j\phi_{p,n}}$), except during deep fades [*e.g.*, see Figs. 10.1(b) and 10.1-(c)]. With any random initialization $\hat{G}_{p,0}$ different from the null vector (here with norm $\sqrt{M}$), $\hat{G}_{p,n}$ indeed converges to the corresponding propagation vector $G_{p,n}$ within a phase ambiguity $\phi_{p,n}$ (*i.e.*, $\hat{G}_{p,n} \simeq e^{-j\phi_{p,n}} G_{p,n}$). The centroid channel ambiguity $a_n$ illustrates the difference between this version of the 2D-STAR and a coherent ST-MRC combiner. As shown in Fig. 10.1, the phase ambiguities $a_{p,n}$ are mutually independent and combine in $a_n$ [see Fig. 10.1(d)] in a destructive manner with parallel/soft DFI, hence the need

for noncoherent temporal differential demodulation and EGC with (10.8) and (10.9).

In fact, the 2D STAR version with parallel/soft DFI readily implements the blind 2D RAKE receiver discussed previously in Sect. 10.3. However, its DFI procedure offers an adaptive PCA implementation that is much more efficient than the iterative PCA method considered in the blind 2D RAKE [8]-[11]. It requires a complexity order per symbol that is only linear in the number of antennas $M$ and it tracks time-varying channels faster due to its LMS-type nature ($\hat{s}_{p,n}$ acts as a reference signal). Furthermore, the iterative PCA method in [8]-[11] is not decision-directed and results in phase ambiguities that are almost random from one block iteration to another. With the DFI procedure, the phase ambiguities $a_{p,n}$ (or $\phi_{p,n}$) can be exploited as "controllable" degrees of freedom to force their convergence to a common constellation-invariant phase rotation (*i.e.*, $r_k \in \mathcal{R}_{\mathcal{M}}$) by both *common* and *hard* signal feedback.

In the following, we explain *hard* then *common* DFI as opposed to *soft* and *parallel* DFI, respectively, then show how combined use of both *common* and *hard* DFI enables implementation of blind quasi-coherent ST-MRC.

### 10.4.3 Parallel and Hard DFI

In a second version of 2D STAR, we implement *parallel* and *hard* DFI in that the feedback signals, still independent (*i.e.*, parallel), now incorporate tentative estimates of the transmitted symbol (*i.e.*, hard) as follows[6]:

$$\hat{s}_{p,n} = \hat{\zeta}_{p,n}\hat{b}_{p,n} = \hat{\varepsilon}_{p,n}\hat{\psi}_n\hat{b}_{p,n}, \tag{10.20}$$

where $\hat{b}_{p,n}$ is the tentative symbol estimate over the $p$-th path given by[7]:

$$\hat{b}_{p,n} = \text{Hard}\left\{\hat{s}_{p,n}\right\} = \underset{c_k \in \mathcal{C}_{\mathcal{M}}}{\arg\min}\left\{|\tilde{s}_{p,n} - c_k|\right\}. \tag{10.21}$$

Previously we have shown that $\tilde{s}_{p,n} \simeq e^{j\phi_{p,n}}s_{p,n} + \eta_{p,n}$ [see (10.7)] with the DFI procedure. Hence, neglecting momentarily $\eta_{p,n}$ in $\tilde{s}_{p,n}$, we have:

$$\hat{b}_{p,n} \simeq \underset{c_k \in \mathcal{C}_{\mathcal{M}}}{\arg\min}\left\{\left|e^{j\phi_{p,n}}s_{p,n} - c_k\right|\right\} = \underset{c_k \in \mathcal{C}_{\mathcal{M}}}{\arg\min}\left\{\left|e^{j\phi_{p,n}}b_n - c_k\right|\right\}. \tag{10.22}$$

Hard decision above exploits the phase ambiguity $a_{p,n} \simeq e^{j\phi_{p,n}}$ as a degree of freedom with $\phi_{p,n} \in [0, 2\pi)$ and hence restricts its realization to limited

[6] An alternative hard feedback signal $\hat{s}_{p,n} = \text{Real}\left\{\tilde{s}_{p,n}\hat{b}^*_{p,n}/|\hat{b}_{p,n}|\right\}\hat{b}_{p,n}/|\hat{b}_{p,n}|$ that performs nearly the same in the DFI procedure of (10.15) finds more efficient use in power estimation (see (10.25)). With $\mathcal{M}$PSK modulations, note that normalization of $\hat{b}_{p,n}$ with $|\hat{b}_{p,n}|$ is not needed [in (10.25) as well].

[7] For non-constant-modulus modulations such as $\mathcal{M}$QAM, minimum distance from constellation $\mathcal{C}_{\mathcal{M}}$ should be found over $|\tilde{s}_{p,n} - \hat{\zeta}_{p,n}c_k|$ in (10.21).

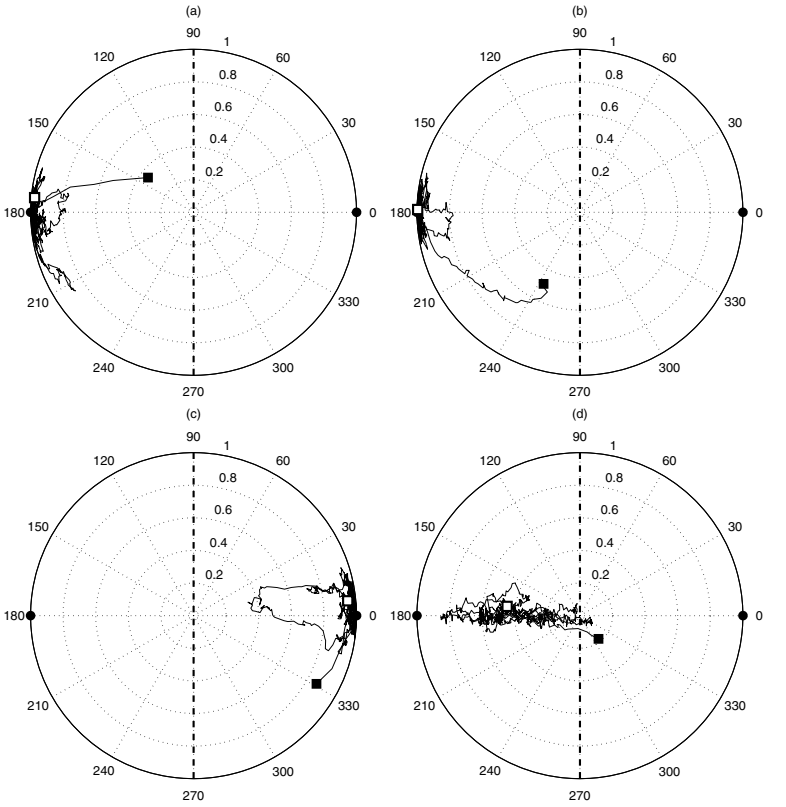


**Fig. 10.2.** Same as Fig. 10.1 with parallel/hard DFI.

constellation-invariant rotation points $r_k \in \mathcal{R}_{\mathcal{M}}$ that minimize the distance between the rotated symbol $e^{j\phi_{p,n}} b_n$ and the constellation $\mathcal{C}_{\mathcal{M}}$. Indeed, we have $r_k b_n \in \mathcal{C}_{\mathcal{M}}$ and hence the minimum distance ideally reduces to zero if we neglect the residual noise contributions in $\tilde{s}_{p,n}$.

Figure 10.2 shows indeed that $a_{p,n}$, with parallel/hard DFI, basically follows the shortest path to the closest rotation point $r_k \in \mathcal{R}_{\mathcal{M}}$ from initial position $a_{p,0}$ in the learning phase then remains in its vicinity after convergence. Hence, the DFI procedure converges with high probability[8] to the following ambiguity over the $p$-th path:

$$a_{p,n} \simeq e^{j\phi_{p,n}} \simeq r_{k(p)} = \underset{r_k \in \mathcal{R}_{\mathcal{M}}}{\arg\min} \left\{ |a_{p,0} - r_k| \right\}. \tag{10.23}$$

[8] Higher perturbations in the DFI procedure due to faster channel variations, higher noise levels or higher adaptation step-size values may prevent $a_{p,n}$ from converging to the closest rotation point in $\mathcal{R}_{\mathcal{M}}$, only to converge to another point in $\mathcal{R}_{\mathcal{M}}$.

Deep fades may sporadically force $a_{p,n}$ away from $r_{k(p)}$ [see Fig. 10.2(c)]. However, amplitude attenuations away from the unit circle are less significant than those observed with parallel/soft DFI (see Fig. 10.2). They suggest that hard DFI has better channel tracking capabilities than soft DFI, by "anchoring" the phase ambiguities to constellation-invariant phase rotations.

With parallel/hard DFI, the ambiguities $a_{p,n} \simeq r_{k(p)}$ are mutually independent and still combine in $a_n$ in a destructive manner as shown in Fig. 10.1(d), hence the need again for noncoherent temporal differential demodulation and EGC with (10.8) and (10.9). For BPSK modulations, however, hard DFI has an advantage over soft DFI. The constellation is one dimensional in the complex plane and the desired signals always lie on the real axis with hard DFI (see Fig. 10.2). Hence for BPSK-modulated hard DFI, noncoherent spatial MRC of (10.7) can be replaced by quasi-coherent (*i.e.*, within a sign ambiguity) spatial MRC as follows:

$$\tilde{s}_{p,n} = \text{Real}\left\{\frac{\hat{G}_{p,n}^H Z_{p,n}}{M}\right\} \simeq \pm s_{p,n} + \text{Real}\{\eta_{p,n}\}. \tag{10.24}$$

This further reduces the residual noise variance by factor 2 and thereby reduces the detection errors (see Sect. 10.4.6) in both (10.8) and (10.9).

Reduction of the residual noise power by factor 2 can be also exploited in enhancing power estimation with hard DFI. However, this improvement can be achieved for both BPSK and higher-order modulations by rewriting (10.11) as:

$$\hat{\zeta}_{p,n+1}^2 = (1-\alpha)\hat{\zeta}_{p,n}^2 + \alpha \text{Real}\left\{\tilde{s}_{p,n}\hat{b}_{p,n}^*/|\hat{b}_{p,n}|\right\}^2. \tag{10.25}$$

Projection of $\tilde{s}_{p,n}$ over the normalized tentative symbol estimate $\hat{b}_{p,n}/|\hat{b}_{p,n}|$ indeed reduces the variance of the residual noise by half and improves estimation[9] of $\hat{\zeta}_{p,n}^2$ above as well as $\hat{\psi}_n^2$ and $\hat{\varepsilon}_{p,n}^2$ in (10.12) and (10.13), respectively.

### 10.4.4 Common and Soft DFI

In a third version of 2D STAR, we implement *common* and *soft* DFI in that the feedback signals are based on weighted replicas of the same (*i.e.*, common) soft output value $\tilde{s}_n$ of noncoherent ST-MRC (*i.e.*, soft):

$$\hat{s}_{p,n} = \hat{\varepsilon}_{p,n}\tilde{s}_n, \tag{10.26}$$

[9] Projection of $\tilde{s}_{p,n}$ over the orthogonal to $\hat{b}_{p,n}/|\hat{b}_{p,n}|$, given by $\text{Im}\left\{\tilde{s}_{p,n}\hat{b}_{p,n}^*/|\hat{b}_{p,n}|\right\}$ [5], [18], enables estimation of the residual noise variance and its subtraction from $\hat{\zeta}_{p,n}^2$ for an even more enhanced power estimation. For simplicity, this option will not be pursued further.

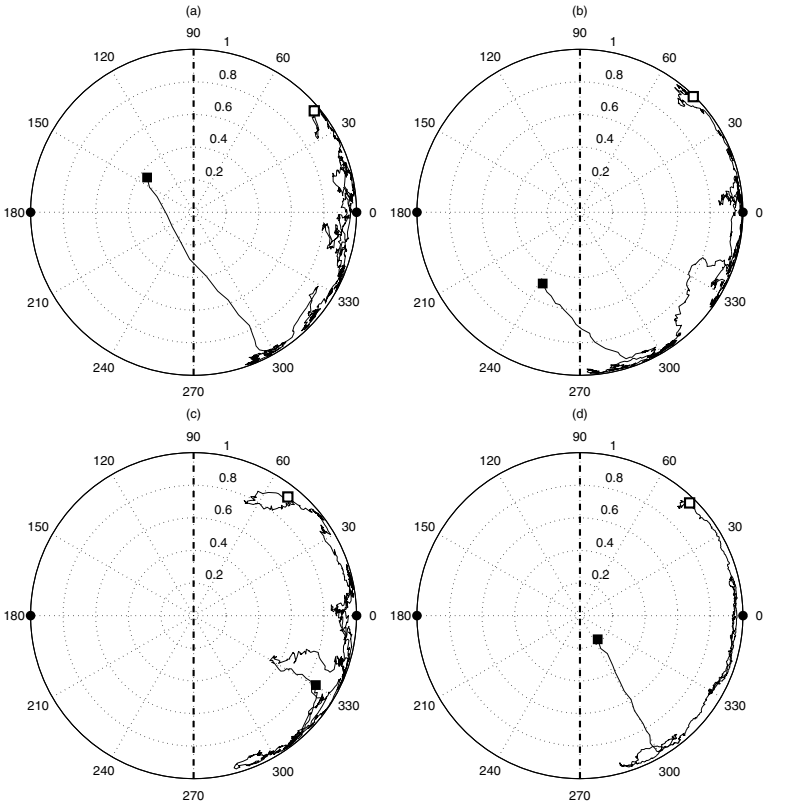


**Fig. 10.3.** Same as Fig. 10.1 with common/soft DFI.

where $\tilde{s}_n$ is simply obtained by noncoherent temporal MRC[10] of the soft outputs $\tilde{s}_{p,n}$ of noncoherent spatial MRC in (10.7):

$$\tilde{s}_n = \sum_{p=1}^{P} \hat{\varepsilon}_{p,n} \tilde{s}_{p,n} = \sum_{p=1}^{P} \hat{\varepsilon}_{p,n} \hat{G}_{p,n} Z_{p,n}/M. \tag{10.27}$$

Exploiting again the expression for $\tilde{s}_{p,n} \simeq e^{j\phi_{p,n}} s_{p,n} + \eta_{p,n}$ [see (10.7)] established with the DFI procedure as well as (10.18) and (10.19), we have:

$$\begin{aligned} \hat{s}_n &= \sum_{p=1}^{P} \hat{\varepsilon}_{p,n} e^{j\phi_{p,n}} s_{p,n} + \left( \sum_{p=1}^{P} \hat{\varepsilon}_{p,n} \eta_{p,n} \right) \qquad (10.28) \\ &= \left( \sum_{p=1}^{P} \hat{\varepsilon}_{p,n} \varepsilon_{p,n} e^{j\phi_{p,n}} \right) \psi_n b_n + \eta_n = a_n s_n + \eta_n = \rho_n e^{j\phi_n} s_n + \eta_n, \end{aligned}$$

[10] Note that estimates of $\hat{\varepsilon}_{p,n}^2$ from (10.13) required for temporal MRC (also used in hard DFI in (10.20)), with no use in the 2D RAKE, definitely enable significant enhancements of 2D receivers in the following.

where the residual output noise $\eta_n$ is Gaussian with variance $\sigma_N^2/M$ since $\hat{\varepsilon}_{p,n}^2$ sum up to 1. Common DFI exploits the phase ambiguities $a_{p,n} \simeq e^{j\phi_{p,n}}$ as degrees of freedom to tie their values after convergence to a unique phase ambiguity $a_n \simeq e^{j\phi_n}$ (*i.e.*, $\rho_n = |a_n| \simeq 1$ and $a_{p,n} \simeq e^{j\phi_{p,n}} \simeq a_n \simeq e^{j\phi_n}$ after convergence), in order to maximize the energy of both $\tilde{s}_n$ and the feedback signal $\hat{s}_{p,n}$ by constructive combining (see another interpretation later in Sect. 10.5.3). Hence we have $\tilde{s}_n \simeq e^{j\phi_n} s_n + \eta_n$, $\tilde{s}_{p,n} \simeq e^{j\phi_n} s_{p,n} + \eta_{p,n}$ and $\hat{G}_{p,n} \simeq e^{-j\phi_n} G_{p,n}$ after convergence.

Figure 10.3 shows indeed that the centroid ambiguity $a_n$ [see Fig. 10.3(d)], with common/soft DFI, follows the shortest path from initial position $a_0$ towards the unit circle in the learning phase, then remains in its vicinity after convergence. Phase deviations around the unit circle are due to the time variations of the channel realizations. After convergence, the multipath ambiguities $a_{p,n}$ are tied together to $a_n$ (see final values of $a_{p,n}$ and $a_n$ nearly at the same position in Fig. 10.3) and hence combine constructively in $a_n$. Amplitude attenuations of $a_n$ away from the unit circle are less significant than those of $a_{p,n}$, themselves weaker than those observed in Fig. 10.1. They suggest that common DFI has better tracking capabilities than soft DFI, by exploiting a "kind" of multipath diversity in the feedback signals.

Noncoherent temporal MRC in (10.27), *a priori* destructive, forces the phases ambiguities $a_{p,n}$ to a common centroid ambiguity $a_n$ after convergence and hence becomes constructive *a posteriori*. With common DFI, we therefore replace noncoherent temporal differential demodulation and EGC in the decision variable of (10.8) by noncoherent ST-MRC in (10.27) followed by differential demodulation:

$$d_n = \tilde{s}_n \tilde{s}_{n-1}^*, \tag{10.29}$$

to reduce detection errors (see Sect. 10.4.6) over the symbol estimate $\underline{\hat{b}}_n$ in (10.9) and possibly enhance data channel-decoding in the case of channel-coded transmissions.

Common DFI has an additional benefit. It can exploit the soft output $\tilde{s}_n$ of noncoherent ST-MRC of (10.27) to directly estimate the total received power as follows:

$$\hat{\psi}_{n+1}^2 = (1-\alpha)\hat{\psi}_n^2 + \alpha|\tilde{s}_n|^2. \tag{10.30}$$

Compared to the two equivalent total-power estimates of (10.10) or (10.12) which sum $P$ squared terms (*i.e.*, temporal EGC), the new estimate sums one squared term only (*i.e.*, noncoherent ST-MRC) and therefore improves power control from weaker variance due to residual noise [20].

### 10.4.5 Common and Hard DFI

In a fourth and last version of 2D STAR, we implement *common* and *hard* DFI in that the feedback signals enclose weighted replicas of the same (*i.e.*,

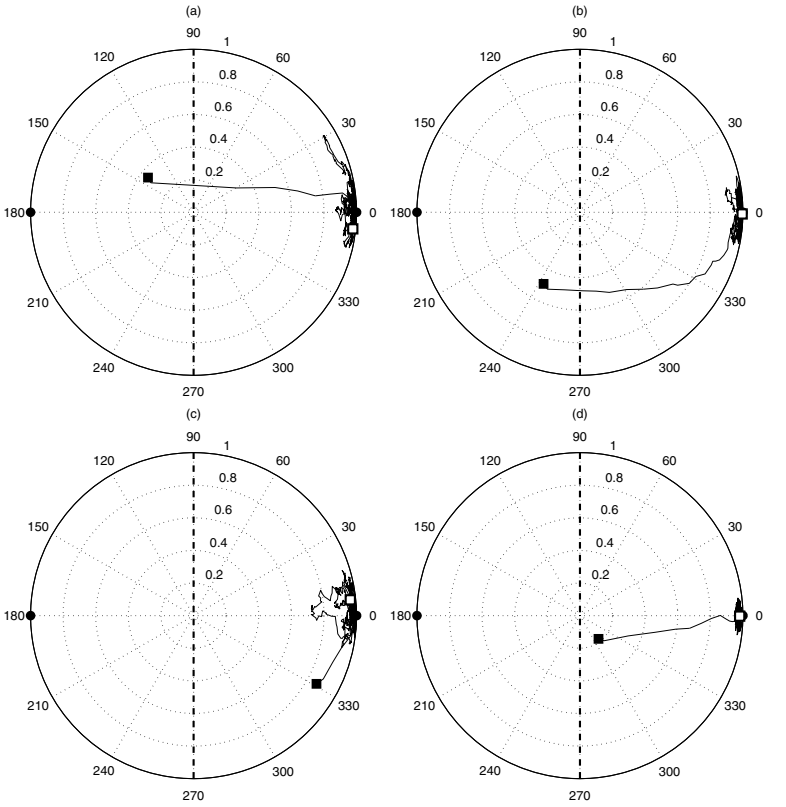


**Fig. 10.4.** Same as Fig. 10.1 with common/hard DFI.

common) tentative symbol estimate (*i.e.*, hard)[11]:

$$\hat{s}_{p,n} = \hat{\zeta}_{p,n}\hat{b}_n = \hat{\varepsilon}_{p,n}\hat{\psi}_n\hat{b}_n, \tag{10.31}$$

where the tentative symbol estimate $\hat{b}_n$ is obtained by hard[12] decision over the soft output $\tilde{s}_n$ of the noncoherent ST-MRC combiner in (10.27):

$$\hat{b}_n = \text{Hard}\{\tilde{s}_n\} = \underset{c_k \in \mathcal{C}_\mathcal{M}}{\arg\min}\{|\tilde{s}_n - c_k|\}. \tag{10.32}$$

[11] An alternative hard feedback signal $\hat{s}_{p,n} = \left|\text{Real}\left\{\tilde{s}_{p,n}\hat{b}_n^*/|\hat{b}_n|\right\}\right| \hat{b}_n/|\hat{b}_n|$ performs nearly the same in the DFI procedure (see footnote 6).

[12] For non-constant-modulus modulations such as $\mathcal{M}$QAM, it is more accurate to find minimum distance from constellation $\mathcal{C}_\mathcal{M}$ over $|\tilde{s}_n - \hat{\psi}_n c_k|$. However, power control attempts to equalize $\psi_n^2$ to 1 and hence the rule in (10.32) holds, unlike (10.21) (see footnote 7).

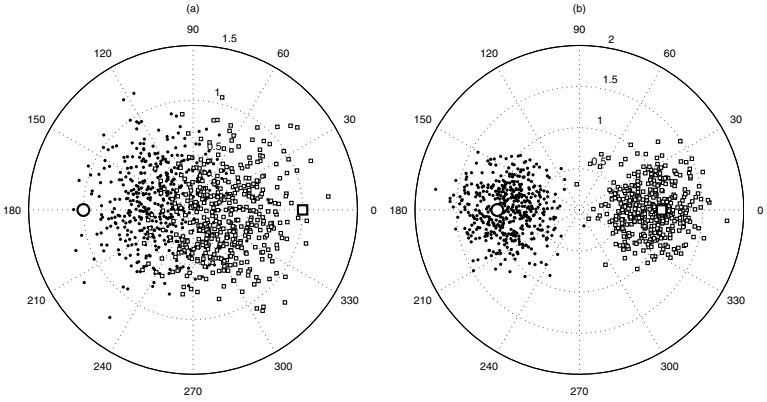


**Fig. 10.5.** Realizations of the noncoherent ST-MRC soft output $\tilde{s}_n$ in (10.27) for (a): common/soft DFI, (b): common/hard DFI. Realizations marked with a small square correspond to the nominal transmitted symbol among the constellation points $c_k \in \mathcal{C}_{\mathcal{M}}$ marked with a large square.

With common/soft DFI, we have just shown that $\tilde{s}_n \simeq e^{j\phi_n} s_n + \eta_n$. Hence, neglecting momentarily $\eta_n$ in $\tilde{s}_n$, we have:

$$\hat{b}_n \simeq \underset{c_k \in \mathcal{C}_{\mathcal{M}}}{\arg\min} \left\{ \left| e^{j\phi_n} s_n - c_k \right| \right\} = \underset{c_k \in \mathcal{C}_{\mathcal{M}}}{\arg\min} \left\{ \left| e^{j\phi_n} b_n - c_k \right| \right\}. \tag{10.33}$$

Hard decision above exploits the centroid phase ambiguity $a_n \simeq e^{j\phi_{p,n}}$ as a degree of freedom with $\phi_n \in [0, 2\pi)$ and hence restricts its realization to limited constellation-invariant rotation points $r_k \in \mathcal{R}_{\mathcal{M}}$ that minimize the distance between the rotated symbol $e^{j\phi_n} b_n$ and the constellation $\mathcal{C}_{\mathcal{M}}$ (see similar discussion below (10.22)). Simultaneously, common DFI ties all multipath phase ambiguities $a_{p,n}$ to $a_n$ and hence $a_{p,n} \simeq a_n \in \mathcal{R}_{\mathcal{M}}$ after convergence.

Figure 10.4 shows indeed that the centroid ambiguity $a_n$, with common/hard DFI, follows the shortest path from initial position $a_0$ to the closest rotation point $r_k \in \mathcal{R}_{\mathcal{M}}$, then remains in its vicinity after convergence. The figure also shows that the multipath phase ambiguities are bound to converge to the same rotation point. Hence, the DFI procedure converges with high probability (see footnote 8) to the following phase ambiguity:

$$a_n = a_{p,n} \simeq e^{j\phi_n} \simeq r_k = \underset{r_k \in \mathcal{R}_{\mathcal{M}}}{\arg\min} \left\{ |a_0 - r_k| \right\}. \tag{10.34}$$

Amplitude attenuations of both $a_{p,n}$ and $a_n$ are significantly weaker than those observed in Figs. 10.1, 10.2, and 10.3 with the previous DFI versions. They suggest that common and hard DFI has better tracking capabilities than parallel and/or soft DFI, 1) by exploiting a "kind" of multipath diversity in the feedback signals, and 2) by "anchoring" all phase ambiguities to a common constellation-invariant phase rotation.

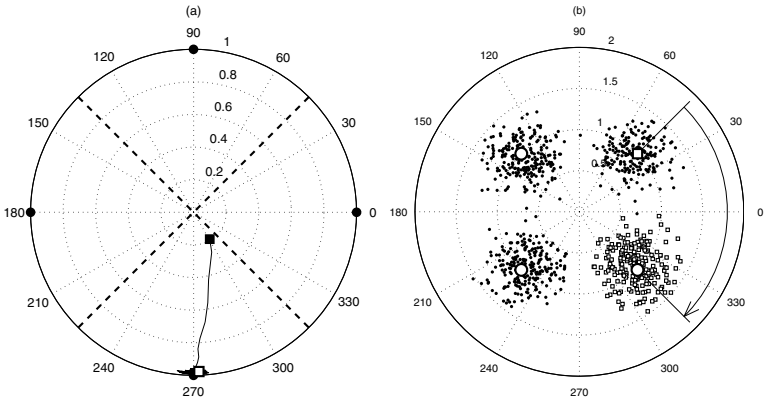


**Fig. 10.6.** (a): Centroid phase ambiguity $a_n$ with QPSK-modulated common/hard DFI (see caption of Fig. 10.1 for additional explanations). (b): Realizations of the noncoherent ST-MRC soft output $\tilde{s}_n$ in (10.27) with QPSK-modulated common/hard DFI (see caption of Fig. 10.5 for additional explanations).

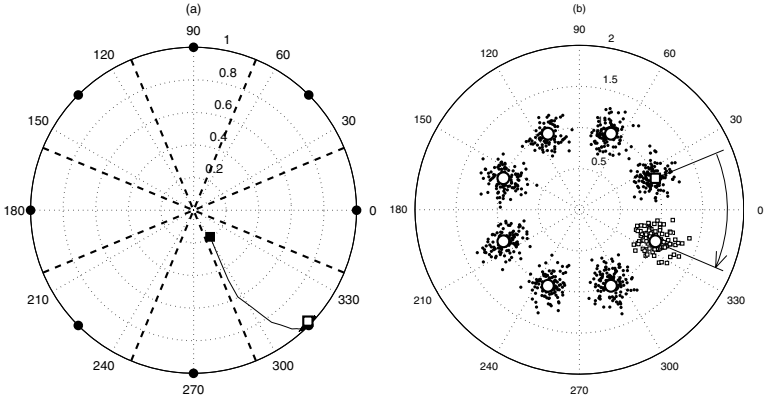


**Fig. 10.7.** Same as Fig. 10.6 with 8PSK modulation instead.

Figure 10.5 shows that common/soft DFI results in a continuous deviation of the ST-MRC output from the constellation points [see Fig. 10.5(a)], while common/hard DFI rotates them back around the nominal constellation points [see Fig. 10.5(b)] within a constellation-invariant phase rotation $r_k$ [$r_k \simeq +1$ only because $a_0$ was closer to $+1$ in Fig. 10.4(d), see (10.34)]. The soft output $\tilde{s}_{p,n}$ of ST-MRC, *a priori* noncoherent with common/soft DFI, becomes *a posteriori* quasi-coherent (*i.e.*, within a constellation-invariant phase rotation) after convergence with common/hard DFI.

This useful "anchoring" mechanism that casts the soft output of ST-MRC around the nominal positions of the constellation points, illustrated so far with BPSK, holds very well with higher-order modulations. With QPSK-modulated common/hard DFI, Fig. 10.6 shows that the centroid phase am-

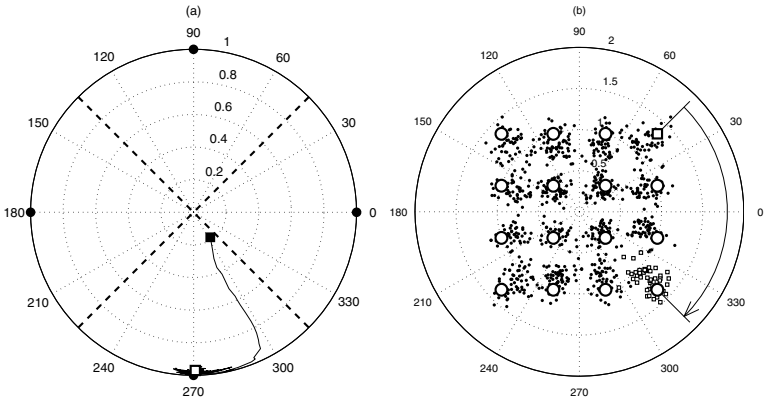


**Fig. 10.8.** Same as Fig. 10.6 with 16QAM modulation instead (normalized constellation with average unit power and $SNR_{\text{in}} = 12$ dB).

biguity $a_n$ converges to the closest rotation point $r_k \in \mathcal{R}_{\mathcal{M}}$ from $a_0$, *i.e.*, $r_k = -j$ [see Fig. 10.6(a)], resulting in a rotation of the ST-MRC output by $-\pi/2$ from nominal constellation points [see Fig. 10.6(b)]. Similar observations can be made from Fig. 10.7 for 8PSK-modulated common/hard DFI where realizations rotated by $-\pi/4$ from nominal positions (*i.e.*, $a_0$ is closer to $r_k = (1-j)/\sqrt{2}$).

In fact, this useful "anchoring" mechanism of common/hard DFI holds even for $\mathcal{M}$QAM modulations as illustrated in Fig. 10.8 with 16QAM. Due to its geometry, 16QAM has the same set $\mathcal{R}_{\mathcal{M}}$ of rotation points $r_k$ as QPSK [see Fig. 10.6(a)]. Hence the centroid phase $a_n$, which starts from the same initial position $a_0$, also converges to $r_k = -j$ as the closest rotation point [see Fig. 10.8(a)], thereby resulting in a rotation of the ST-MRC output by $-\pi/2$ from nominal constellation points [see Fig. 10.8(b)]. With standard $\mathcal{M}$QAM modulations, however, there is no trivial differential coding scheme[13] to alleviate a channel phase ambiguity even if the phase rotation is constellation-invariant. The phase "anchoring" mechanism of $\mathcal{M}$QAM-modulated common/hard DFI finds particularly good application later with pilot-assisted versions of STAR (see Sects. 10.6 and 10.6.6).

With $\mathcal{M}$PSK modulations, differential coding at transmission enables detection of symbols with a channel phase ambiguity. We resolve it by noncoherent ST-MRC and differential demodulation at the receiver when equipped with common/soft DFI [see (10.27) and (10.29)]. With common/hard DFI, however, the soft output $\tilde{s}_n$ of ST-MRC becomes quasi-coherent (*i.e.*, within a constellation-invariant phase rotation) and hence enables reliable estimation of the transmitted D$\mathcal{M}$PSK symbol $b_n$ from the tentative symbol $\hat{b}_n \simeq r_k b_n$

[13] Differential detection is possible for instance with a star 16QAM constellation, a combination of two 8PSK constellations with different amplitudes (*e.g.*, see [22]).

of (10.32) within a rotation $r_k \in \mathcal{R}_{\mathcal{M}}$. Therefore, power estimation in (10.30) can be replaced by:

$$\hat{\psi}_{n+1}^2 = (1-\alpha)\hat{\psi}_n^2 + \alpha \text{Real}\left\{\tilde{s}_n \hat{b}_n^* / |\hat{b}_n|\right\}^2, \tag{10.35}$$

for improved power estimation and control[14]. Additionally, instead of differential demodulation in (10.29) and hard decision in (10.9), differential decoding of $\hat{b}_n$ enables simple estimation of the $\mathcal{M}$PSK symbol $\underline{b}_n$ as follows:

$$\underline{\hat{b}}_n = \hat{b}_n \hat{b}_{n-1}^* e^{j(1-\delta(\mathcal{M}-2))\pi/\mathcal{M}}. \tag{10.36}$$

Detection errors over $r_k b_n$ in $\hat{b}_n$ of (10.32) (*i.e.*, Prob$[\hat{b}_n \neq r_k b_n]$) are those of coherent ST-MRC, much fewer than those resulting from noncoherent ST-MRC with common/soft DFI. Differential decoding as in (10.36) doubles these errors, yet common/hard DFI significantly outperforms common/soft DFI in symbol detection (see Sect. 10.4.6). For channel-coded transmissions with soft channel decoding, however, we need to pass on the soft decision variable $d_n$ of (10.29) to the decoder. In this case, the performance gains after channel decoding are theoretically those of common/soft DFI. Recent simulations yet suggest that the "anchoring" mechanism of common/hard DFI enables noticeable improvement from limiting phase deviations in $d_n$. This issue is however out of the scope of this contribution.

In the following, we compare the SER (symbol error rate) performance of the four DFI versions discussed previously.

### 10.4.6 Performance Gains of the DFI Versions

Simple analytical expressions for SER (*i.e.*, Prob$[\underline{\hat{b}}_n \neq \underline{b}_n]$) can be derived only for BPSK with differential demodulation and for $\mathcal{M}$PSK with differential decoding, both over Gaussian channels (see general closed-form expressions in [23], [24] for instance). Here, in Fig. 10.9, we simply plot the SER curves obtained by simulations for each DFI version when modulated with BPSK, QPSK, and 8PSK. These curves confirm the performance gains expected from successive upgrades of the DFI procedure in 2D STAR.

As shown in Fig. 10.9, the 2D STAR version with parallel/soft DFI, which better approximates the blind 2D RAKE receiver (see Sects. 10.3 and 10.4.2), performs worst. Parallel/hard DFI outperforms parallel/soft DFI only with BPSK where noncoherent spatial MRC in (10.7) is replaced by quasi-coherent spatial MRC in (10.24). Common/soft DFI always outperforms parallel/soft

[14] Similarly to (10.25), projection of $\tilde{s}_n$ over 1) the normalized tentative symbol estimate $\hat{b}_n/|\hat{b}_n|$ and 2) over its orthogonal, given by Im$\left\{\tilde{s}_n \hat{b}_n^*/|\hat{b}_n|\right\}$ [5], [18], 1) reduces the variance of the residual noise by half in (10.35), and 2) enables estimation of this variance then its subtraction from $\hat{\psi}_n^2$ for an even more enhanced power estimation (see footnote 9).

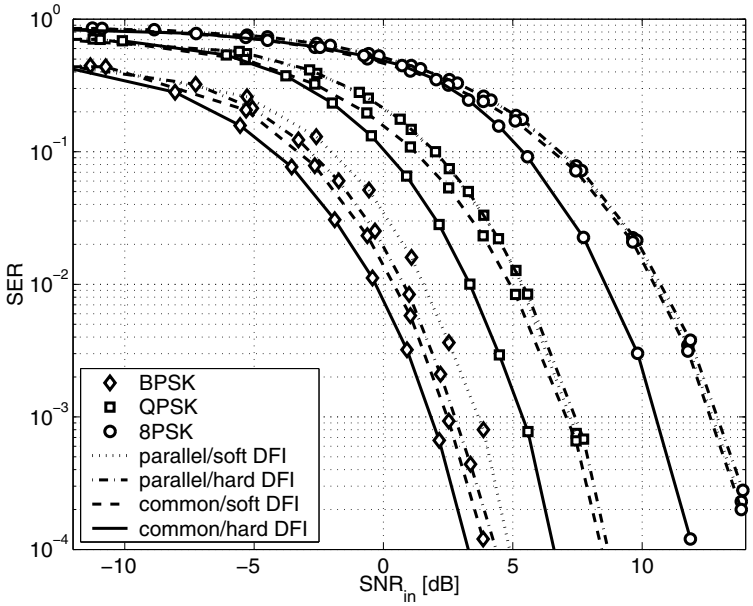


**Fig. 10.9.** SER vs. SNR in dB of blind 2D STAR with various $\mathcal{M}$PSK modulated-DFI versions using optimum step-size $\mu_{p,\mathrm{opt}}\left(\bar{\varepsilon}_p^2\bar{\psi}^2, \sigma_N^2, f_D T_s\right)$ in (10.52) (see Sect. 10.5.4).

DFI by replacing noncoherent temporal differential demodulation and EGC in (10.8) by noncoherent temporal MRC in (10.27) and differential demodulation in (10.29). The SNR gain however shrinks steadily as the modulation is changed from BPSK to higher order. Common/soft DFI even outperforms parallel/hard DFI with BPSK, suggesting that gains from noncoherent temporal MRC vs. EGC are more significant than those of quasi-coherent vs. noncoherent spatial MRC. Common/hard DFI outperforms all other DFI versions by implementing quasi-coherent ST-MRC. Regardless of the modulation employed, its offers an SNR gain of about 2 dB over the worst DFI version, *i.e.*, parallel/soft DFI which better approximates the blind 2D RAKE receiver.

Overall, we have been able to upgrade the blind 2D RAKE by introducing incremental improvements to the combining operation thereby enabling the blind 2D STAR to gain about 2 dB in SNR over blind 2D RAKE-type receivers with all tested $\mathcal{M}$PSK modulations.

## 10.5 The Blind 1D-ST STAR

So far, we have exploited the flexibility of the DFI procedure in a 2D structured receiver, *i.e.*, sequential processing of diversity fingers in two dimen-

sions: first in space over antennas then in time over multipaths. Ultimately, we arrive at a quasi-coherent ST-MRC combiner in 2D STAR with common and hard DFI. Yet by exploiting the *common* DFI version, further improvements are achievable by 1) identifying then 2) combining all diversity fingers jointly in space and time with 1D-ST (space-time) structured versions of STAR. Of particular interest, the 1D-ST counterpart of the 2D structured STAR with common and hard DFI, implements quasi-coherent joint ST-MRC with reduced complexity, increased robustness to changing propagation conditions, and increased accuracy and speed of channel estimation.

### 10.5.1 1D-ST Structured Data Model

Let us simply align the multipath despread vectors $Z_{p,n}$ for $p = 1, \ldots, P$ in an $MP \times 1$ spatio-temporal despread vector [see (10.6)]:

$$\underline{Z}_n = \begin{bmatrix} Z_{1,n} \\ \vdots \\ Z_{p,n} \\ \vdots \\ Z_{P,n} \end{bmatrix} = \begin{bmatrix} \varepsilon_{1,n} G_{1,n} \\ \vdots \\ \varepsilon_{p,n} G_{p,n} \\ \vdots \\ \varepsilon_{P,n} G_{P,n} \end{bmatrix} \psi_n b_n + \begin{bmatrix} N_{1,n} \\ \vdots \\ N_{p,n} \\ \vdots \\ N_{P,n} \end{bmatrix} = \underline{H}_n s_n + \underline{N}_n, \qquad (10.37)$$

where $s_n = \psi_n b_n$ is the signal component, $\underline{H}_n$ is the $MP \times 1$ spatio-temporal propagation vector and $\underline{N}_n$ is the $MP \times 1$ zero-mean uncorrelated spatio-temporal Gaussian noise vector with covariance matrix $\mathbf{R}_{\underline{N}} = \sigma_N^2 \mathbf{I}_{MP}$.

This 1D-ST structured data model is actually a simplification of the post-correlation model (PCM) introduced in [4] to efficiently address the more general issue of joint space-time processing with simultaneous multipath time-delay synchronization in STAR. Exploitation of a similar 1D-ST structured data model before despreading later allowed development of very efficient multi-user upgrades of STAR by simultaneous joint-space-time signal combining, channel identification, time-delay synchronization and interference suppression [7]. To our knowledge, the advantages of simultaneous joint space-time processing operations were not recognized previously and were not pursued to further integrate the spatial dimension made available by antenna-arrays (see discussion in [7] and references therein). Below we exhibit the advantages of joint space-time signal combining and channel identification using the simplified 1D-ST structured data model above.

### 10.5.2 2D STAR with Common DFI Reinterpreted

Common DFI enables exploitation of the 1D-ST data model of (10.37) in 1) reformulating the two sequential spatial and temporal processing steps of 2D STAR in a compact form, 2) reinterpreting the resulting compact form as a joint space-time processing step, and 3) reimplementing this joint space-time processing step in a more efficient 1D-ST structure of STAR.

Using the expressions for $Z_{p,n}$, $a_{p,n}$ and $a_n$ in (10.6), (10.18), and (10.19), respectively, we further analyze the expression for the soft output $\tilde{s}_n$ of noncoherent ST-MRC in (10.27) as shown in the upward developments of the following equation:

$$\tilde{s}_n = \left\{ \begin{array}{c} a_n s_n + \eta_n \\ \uparrow \\ \left( \sum_{p=1}^{P} \hat{\varepsilon}_{p,n} \varepsilon_{p,n} a_{p,n} \right) s_n + \left( \sum_{p=1}^{P} \hat{\varepsilon}_{p,n} \eta_{p,n} \right) \\ \uparrow \\ \left( \sum_{p=1}^{P} \hat{\varepsilon}_{p,n} \varepsilon_{p,n} \hat{G}_{p,n}^H G_{p,n}/M \right) s_n + \left( \sum_{p=1}^{P} \hat{\varepsilon}_{p,n} \hat{G}_{p,n}^H N_{p,n}/M \right) \\ \downarrow \\ \underline{\hat{H}}_n^H \underline{Z}_n/M \\ \downarrow \\ \left( \underline{\hat{H}}_n^H \underline{H}_n/M \right) s_n + \left( \underline{\hat{H}}_n^H \underline{N}_n/M \right) \end{array} \right. . \quad (10.38)$$

In the downward developments, however, we can reformulate $\tilde{s}_n$ as the soft output of the space-time propagation vector estimate $\underline{\hat{H}}_n$ combining the space-time despread vector $\underline{Z}_n$ by ST-MRC, noncoherent or quasi-coherent depending on whether soft or hard DFI was used jointly with common DFI.

Exploiting the 1D-ST structured data model of (10.37) and equating the developments above allows reinterpretation of the two sequential spatial then temporal MRC combining steps of (10.7) and (10.27) (*i.e.*, 2D structured) as a single joint ST-MRC combining step (*i.e.*, 1D-ST structured). Additionally, the centroid channel ambiguity $a_n$ of (10.19) can be considered as the normalized scalar product $\underline{\hat{H}}_n \underline{H}_n/M$ that measures the total distortion between the space-time propagation vector $\underline{H}_n$ and its estimate $\underline{\hat{H}}_n$. The above reinterpretations of the processing steps in 2D STAR with common DFI along the 1D-ST data model call for directly estimating the space-time propagation vector $\underline{H}_n$ in a single joint space-time identification step using 1D-ST structured DFI.

### 10.5.3 1D-ST Structured DFI

Driven by the same channel estimates as 2D-STAR with common DFI, joint space-time processing suggests merely simple rearrangements of the data structure processed sequentially in space then in time. The 2D and 1D-ST structured STAR versions would be identical and would have the same performance. Actually, the benefits of joint spatio-temporal processing go beyond compact spatio-temporal data modeling when they reach the steps of signal combining and channel identification. Indeed, joint space-time processing replaces the $P$ disjoint DFI procedures of (10.15) for all paths, referred to as

2D structured DFI, by a single joint spatio-temporal DFI update[15]:

$$\hat{\underline{H}}_{n+1} = \hat{\underline{H}}_n + \mu \left( \underline{Z}_n - \hat{\underline{H}}_n \hat{s}_n \right) \hat{s}_n^*, \tag{10.39}$$

where $\mu$ is an adaptation step-size, and the common feedback signal $\hat{s}_n$ is a selected estimate of the spatio-temporal signal component. As shown later in Sect. 10.5.4, this 1D-ST structured DFI procedure outperforms its 2D structured counterpart by reducing channel estimation and power control errors.

A first version of 1D-ST STAR transforms 2D structured common/soft DFI (see Sect. 10.4.4) into 1D-ST structured soft DFI using the following feedback signal in (10.39):

$$\hat{s}_n = \tilde{s}_n, \tag{10.40}$$

where the soft output $\tilde{s}_n$ of joint noncoherent ST-MRC:

$$\tilde{s}_n = \hat{\underline{H}}_n^H \underline{Z}_n / M, \tag{10.41}$$

replaces that obtained by (10.27). Estimation of the total received power $\hat{\psi}_n^2$, the decision variable $d_n$ and the $\mathcal{M}$PSK data symbol $\hat{\underline{b}}_n$ follow using (10.35), (10.29), and (10.9), respectively.

Substituting $\tilde{s}_n$ for $\hat{s}_n$ in (10.41), the 1D-structured DFI procedure can be rewritten as [see (10.17)]:

$$\begin{aligned} \hat{\underline{H}}_{n+1} &= \hat{\underline{H}}_n + \mu \left( \underline{Z}_n - \hat{\underline{H}}_n \hat{\underline{H}}_n^H \underline{Z}_n / M \right) \underline{Z}_n^H \hat{\underline{H}}_n / M \\ &= \hat{\underline{H}}_n + \mu \left( \mathbf{I}_{MP} - \hat{\underline{H}}_n \hat{\underline{H}}_n^H / M \right) \underline{Z}_n \underline{Z}_n^H \hat{\underline{H}}_n / M \\ &= \hat{\underline{H}}_n + \mu \mathbf{\Pi}_n \dot{\mathbf{R}}_{\underline{Z}} \hat{\underline{H}}_n / M, \end{aligned} \tag{10.42}$$

and its adaptation gradient interprets as a projector $\mathbf{\Pi}_n$ orthogonal to $\hat{\underline{H}}_n$ of $\dot{\mathbf{R}}_{\underline{Z}}$, the instantaneous estimate of the correlation matrix $\mathbf{R}_{\underline{Z}}$ of $\underline{Z}_n$ [see (10.14)]:

$$\mathbf{R}_{\underline{Z}} = \bar{\psi}^2 \left( \underline{H}_n e^{-j\phi_n} \right) \left( \underline{H}_n e^{-j\phi_n} \right)^H + \sigma_N^2 \mathbf{I}_{MP}. \tag{10.43}$$

On average, adaptation errors are minimized when the projector $\mathbf{\Pi}_n$ suppresses the dimension of $\mathbf{R}_{\underline{Z}}$ with the highest energy, *i.e.*, its principal eigenvector $e^{-j\phi_n} \underline{H}_n$ (note that $\mathbf{\Pi}_n \mathbf{R}_{\underline{Z}} \underline{H}_n = \mathbf{\Pi}_n \times (\lambda \underline{H}_n) = 0$ if $\hat{\underline{H}}_n = \lambda' \underline{H}_n$). This new interpretation of the 1D-ST DFI procedure as an adaptive PCA implementation provides a more intuitive justification as to why the multipath ambiguities $a_{p,n}$ are tied, converging in parallel with the centroid ambiguity

[15] Preferably $\|\hat{\underline{H}}_n\|$ is forced to $\sqrt{M}$ after each DFI update for increased stability (we do so in this work), although normalization of $\hat{\underline{H}}_n$ to $\sqrt{M}$ is asymptotically guaranteed after convergence (see footnote 5).

$a_n$ to the same phase ambiguity with common DFI (see discussion below (10.28)).

A second version of 1D-ST STAR transforms 2D structured common/hard DFI (see Sect. 10.4.5) into 1D-ST structured hard DFI using the following feedback signal[16] in (10.39):

$$\hat{s}_n = \hat{\psi}_n \hat{b}_n, \tag{10.44}$$

where the tentative symbol estimate $\hat{b}_n$ is estimated in (10.32) by hard decision over $\tilde{s}_n$ of (10.41). Estimation of the total received power $\hat{\psi}_n^2$ and the decision variable $d_n$ follow by (10.35) and (10.29), respectively. Since 1D-ST hard DFI implements joint quasi-coherent ST-MRC by forcing the centroid channel ambiguity to converge to a constellation-invariant rotation point $r_k \in \mathcal{R}_{\mathcal{M}}$, the $\mathcal{M}$PSK data symbol $\underline{b}_n$ is directly estimated by differential decoding of $\hat{b}_n$ in (10.36). As discussed previously in Sect. 10.4.5, common/hard DFI in 1D-ST hard DFI outperforms common/soft DFI in 1D-ST soft DFI by significantly reducing detection errors over the data symbols $\underline{b}_n$ (see Sect. 10.4.6). Theoretically, they perform equally over channel-coded transmissions although current investigations suggest that the "anchoring" mechanism in hard DFI reduces channel decoding errors (see Sect. 10.4.5).

In the case of a single path (*i.e.*, $P = 1$ in nonselective fading) the 1D-ST and 2D STAR versions become identical when both implement either hard or soft DFI. In the case of a single receive antenna (*i.e.*, $M = 1$ on the downlink for instance), the differences between all the 1D and 2D versions of STAR persist and offer the same potential improvements[17]. We have shown in Sect. 10.4.6 that common/hard DFI outperforms all other versions of 2D STAR by implementing quasi-coherent ST-MRC. Hence next we only compare this 2D version of STAR with its 1D-ST counterpart to show the performance advantages of the latter.

### 10.5.4 Performance Gains of 1D-ST STAR over 2D STAR

We establish below a theoretical performance result that channel identification errors with 1D-ST STAR are smaller than those with 2D-STAR. To

[16] An alternative hard feedback signal $\hat{s}_n = \text{Real}\left\{\tilde{s}_n \hat{b}_n^* / |\hat{b}_n|\right\} \hat{b}_n / |\hat{b}_n|$ that performs nearly the same in the DFI procedure of (10.39) finds more efficient use in power estimation [see (10.35)].

[17] Note in this case that the 1D-ST DFI version amounts to identifying the multipath fades as a temporal channel vector. Similarly, the 2D DFI versions, applied here to the identification of spatial propagation vectors $G_{p,n}$, could easily be combined with another "temporal" DFI procedure applied to the soft outputs $\tilde{s}_{p,n}$ of (10.7) aligned as a temporal observation vector for identification there of $\varepsilon_{p,n} e^{j\phi_{p,n}}$ as a temporal $P \times 1$ channel vector with norm 1. This option is beyond the scope of this contribution. It shows however that 1D-ST DFI amounts to jointly applying two DFI procedures, one in space and another in time.

our knowledge, this is the first analytical explanation as to when and why joint space-time processing outperforms sequential space and time processing. Later we validate this proof by simulations and show the resulting performance advantage of 1D-ST STAR over 2D STAR and current 2D RAKE-type receivers.

We define the mean square error per diversity branch of channel identification in both space and time, referred to in the following as misadjustment, as [17]:

$$\beta^2 = \frac{E\left[\|\Delta \underline{H}_n\|^2\right]}{MP} = \frac{E\left[\|\hat{\underline{H}}_n - \underline{H}_n\|^2\right]}{MP}. \tag{10.45}$$

In [17] we carried out a detailed convergence and performance analysis of channel misadjustment using the 1D-ST structured DFI of (10.39). Here we provide a summary of the main analytical results derived there. We show that the DFI procedure converges in the mean square sense with the following time constant [17]:

$$\tau = \frac{1}{2\mu\bar{\psi}^2\left(1-\frac{\mu\bar{\psi}^2}{2}\right)} \simeq \frac{1}{2\mu\bar{\psi}^2}, \tag{10.46}$$

and establish the analytical expression for steady-state (*i.e.*, after convergence) misadjustment [17]:

$$\beta^2\left(\bar{\psi}^2, \sigma_N^2, f_D T_s, P, \mu\right) = \frac{\mu\sigma_N^2}{2\left(1-\frac{\mu\bar{\psi}^2}{2}\right)} + \frac{2}{P}\left[1-\mathcal{B}_0\left(\frac{2\pi f_D T_s}{\mu\bar{\psi}^2}\right)\right], \tag{10.47}$$

where $\mathcal{B}_0(x)$ is the Bessel function of the first kind of order 0. This expression for misadjustment reflects two contributions, the first from noise, increases with larger values of the adaptation step-size $\mu$ due to higher gradient update perturbations. And the second, from the Doppler spread, increases with smaller values of $\mu$ due to slower tracking of the channel variations. We hence establish the following analytical expressions for the optimum step-size and the resulting minimum misadjustment [19] and time constant (not necessarily the smallest):

$$\mu_{\text{opt}}\left(\bar{\psi}^2, \sigma_N^2, f_D T_s, P\right) = 2\left[\left(\pi f_D T_s\right) / \left(\sqrt{P}\bar{\psi}^2\sigma_N\right)\right]^{\frac{2}{3}}, \tag{10.48}$$

$$\beta^2_{\min}\left(SNR_{\text{in}}, f_D T_s, P\right) = \frac{3}{2}\left[\left(\pi f_D T_s\right) / \left(\sqrt{P} SNR_{\text{in}}\right)\right]^{\frac{2}{3}}, \tag{10.49}$$

$$\tau_{\text{opt}}\left(SNR_{\text{in}}, f_D T_s, P\right) \simeq \frac{1}{4}\left[\sqrt{P} / \left(\pi f_D T_s \sqrt{SNR_{\text{in}}}\right)\right]^{\frac{2}{3}}. \tag{10.50}$$

To the best of our knowledge, these expressions (which apply to reference-assisted receivers as well, see Sect. 10.6) are the first to provide practical means for optimal tuning of adaptive channel identification and for prediction

of step-size, misadjustment and convergence time in a multipath Rayleigh fading environment.

We exploit the theoretical results above to compare the minimum misadjustments and the corresponding time constants of 1D-ST and 2D STAR denoted by $\beta^2_{1D,\min}$, $\tau_{1D,\text{opt}}$, $\beta^2_{2D,\min}$ and $\tau_{2D,\text{opt}}$, respectively. We already have $\beta^2_{1D,\min} = \beta^2_{\min}$ in (10.49) and $\tau_{1D,\text{opt}} = \tau_{\text{opt}}$ in (10.50). For 2D-STAR we derive the expression for $\beta^2_{2D,\min}$ as follows:

$$\beta^2_{2D,\min} = \frac{E\left[\|\hat{\underline{H}}_n - \underline{H}_n\|^2\right]}{MP} = \frac{E\left[\sum_{p=1}^{P} \|\hat{\varepsilon}_{p,n}\hat{G}_{p,n} - \varepsilon_{p,n}G_{p,n}\|^2\right]}{MP}$$
$$= \sum_{p=1}^{P} \frac{\bar{\varepsilon}_p^2}{P} \frac{E\left[\|\Delta G_{p,n}\|^2\right]}{M} + \frac{1}{P}\sum_{p=1}^{P} E\left[|\Delta\varepsilon_{p,n}|^2\right], \tag{10.51}$$

where $\Delta G_{p,n} = \hat{G}_{p,n} - G_{p,n}$ and $\Delta\varepsilon_{p,n} = \hat{\varepsilon}_{p,n} - \varepsilon_{p,n}$ denote the estimation errors over $G_{p,n}$ and $\varepsilon_{p,n}$, respectively, both assumed independent.

Although the analytical expressions of (10.46) to (10.49) assume perfect equalization of the total received power (*i.e.*, $\psi_n^2 = \bar{\psi}^2$) [17], we apply them to 2D DFI with step-size optimization assuming a constant received power over each path $\bar{\varepsilon}_p^2\bar{\psi}^2$ and therefore have:

$$\mu_{p,\text{opt}}\left(\bar{\varepsilon}_p^2\bar{\psi}^2, \sigma_N^2, f_D T_s\right) = 2\left[(\pi f_D T_s) \,/\, \left(\bar{\varepsilon}_p^2\bar{\psi}^2\sigma_N\right)\right]^{\frac{2}{3}} = \frac{P^{\frac{1}{3}}}{\bar{\varepsilon}_p^{\frac{4}{3}}}\mu_{\text{opt}}, \tag{10.52}$$

yielding:

$$\frac{E\left[\|\Delta G_{p,n}\|^2\right]}{M} = \beta^2_{\min}\left(\bar{\varepsilon}_p^2 SNR_{\text{in}}, f_D T_s, 1\right) = \frac{P^{\frac{1}{3}}}{\bar{\varepsilon}_p^{\frac{4}{3}}}\beta^2_{1D,\min}. \tag{10.53}$$

Using the expression above in (10.51), we have:

$$\beta^2_{2D,\min} = \left[\sum_{p=1}^{P} \frac{1}{P}\left(\bar{\varepsilon}_p^2 P\right)^{\frac{1}{3}}\right]\beta^2_{1D,\min} + \beta^2_{\varepsilon} = \kappa\beta^2_{1D,\min} + \beta^2_{\varepsilon}, \tag{10.54}$$

where $\beta^2_{\varepsilon}$ denotes the average estimation errors over multipath amplitudes given by the second summation term in (10.51). Theory provides bounds to the factor $\kappa$ between 0 and 1. With realistic average multipath power profiles[18], however, values for $\kappa$ are actually close to 1 so that in practice we have:

$$\beta^2_{2D,\min} \simeq \beta^2_{1D,\min} + \beta^2_{\varepsilon} > \beta^2_{1D,\min}. \tag{10.55}$$

[18] With equal-power paths (*i.e.*, $\bar{\varepsilon}_p^2 = 1/P$), note that a feedback signal with average power $\bar{\psi}^2/P$ in 2D DFI yields $\mu_{p,\text{opt}} = P\mu_{\text{opt}}$ and $E\left[\|\Delta G_{p,n}\|^2\right]/M = P\beta^2_{1D,\min}$ in (10.52) and (10.53), respectively. In (10.54), note also that $\kappa = 1$ and $\beta^2_{2D,\min} = \beta^2_{1D,\min} + \beta^2_{\varepsilon}$.

This steady-state misadjustment is reached after convergence with a time constant dominated by the weakest multipath power, say $\bar{\varepsilon}^2_{\min}$:

$$\tau_{2D,\text{opt}} \simeq \tau_{\text{opt}} \left(\bar{\varepsilon}^2_{\min} SNR_{\text{in}}, f_D T_s, 1\right) \simeq \frac{1}{(\bar{\varepsilon}^2_{\min} P)^{\frac{1}{3}}} \tau_{1D,\text{opt}} \geq \tau_{1D,\text{opt}}. \quad (10.56)$$

Intuitively, a joint 1D-ST DFI update with the total received power in the feedback signal $\hat{s}_n$ of (10.39) results in 1) less misadjustment and 2) faster convergence than separate 2D DFI updates with fractioned and possibly unbalanced[19] powers in the multipath feedback signals $\hat{s}_{p,n}$ of (10.15). Additionally, a joint 1D-ST DFI update estimates the multipath amplitudes $\varepsilon_{p,n}$ implicitly in the space-time channel estimate $\underline{\hat{H}}_n$ and hence avoids the additional misadjustment $\beta^2_\varepsilon$ in (10.55) that arises inevitably with separate 2D DFI updates regardless of the multipath amplitude estimation technique employed (see footnote 17).

To our knowledge, the theoretical results above provide the first analytical explanation as to when and why joint space-time processing outperforms sequential space and time processing widely implemented today in RAKE-type receivers (see Sect. 10.3). We illustrate them below by simulations with focus on the minimum misadjustment and the resulting SER.

In Fig. 10.10(a) we plot the minimum misadjustment for the 1D-ST and 2D versions of STAR using the corresponding optimum step-sizes. To widen the scope of comparisons between the 1D-ST and 2D versions of STAR, we increase the Doppler up to about 90 Hz (*i.e.*, speed of 50 Kmph) in Fig. 10.10(b). For both low and high Doppler, misadjustment curves in Fig. 10.10 show a very good fit between the theoretical and experimental values of $\beta^2_{1D,\min}$ in (10.49) with 1D-ST STAR. They also suggest that analytical expressions of (10.46) to (10.49) derived for BPSK in [17], [19] hold for higher-oder modulations as well, the fit to the experimental curves improving at even higher SNR values. More importantly, the misadjustment curves confirm the theoretical proof of (10.55) above that indeed 2D STAR performs worse in channel identification than 1D-ST STAR, the gap in misadjustment being larger at faster Doppler.

Nevertheless, reduction of misadjustment in Fig. 10.10 is not sufficient to result in a noticeable SER reduction in Fig. 10.11, especially at lower SNR where the gap in misadjustment between 1D-ST and 2D STAR is smaller. This suggests that 1D-ST STAR performs nearly the same in SER as 2D STAR over a large range of Doppler despite gains in minimum misadjustment achieved with optimum step-sizes. However, the little gap that appears between the SER curves in Fig. 10.11(b) suggests that noticeable SNR gains can be expected with 1D-ST STAR at very high Doppler, especially at high SNR and with higher-order modulations.

[19] With equal-power paths (*i.e.*, $\bar{\varepsilon}^2_p = \bar{\varepsilon}^2_{\min} = 1/P$), we have $\tau_{2D,\text{opt}} \simeq \tau_{1D,\text{opt}}$ in (10.56). With unbalanced multipath power profiles, 2D DFI is hence slower. Furthermore, simulations indicate that it produces even higher misadjustment.

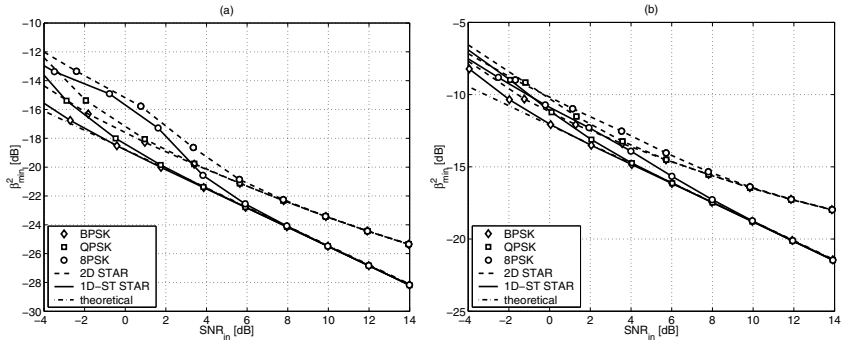


**Fig. 10.10.** Minimum misadjustment in dB vs. SNR in dB for 1D-ST and 2D STAR with $\mathcal{M}$PSK modulations and optimum step-sizes $\mu_{\rm opt}$ and $\mu_{p,\rm opt}$ of (10.48) and (10.52), respectively. (a): Doppler of 9 Hz. (b): Doppler increased up to 90 Hz.

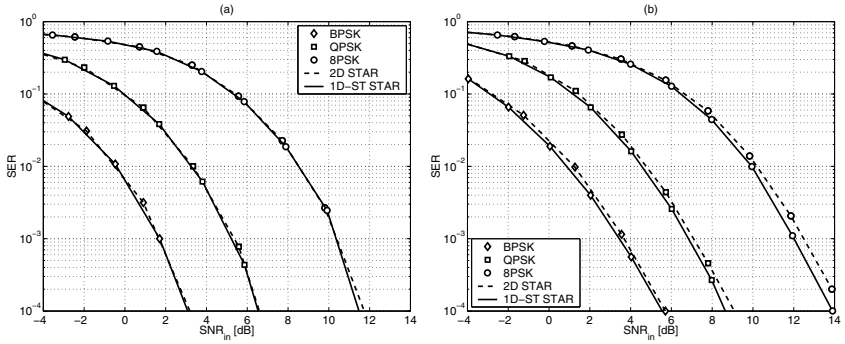


**Fig. 10.11.** Same as Fig. 10.10 with SER vs. SNR in dB instead.

**Table 10.2** Complexity per symbol for the 2D and 1D-ST versions of STAR.

| operation | $. + .$ | $. \times .$ | $./.$ | $\sqrt{.}$ |
|---|---|---|---|---|
| number of operations (complex for $+$, $\times$ and $/$) | | | | |
| 2D STAR | $3MP + 2P - 2$ | $3MP + 5P + 1$ | $MP + 2P$ | $2P + 1$ |
| 1D-ST STAR | $3MP$ | $3MP + 5$ | $MP + 1$ | 2 |
| reduction in number of operations with joint processing | | | | |
| $M = 4, P = 3$ | 10% | 20% | 30% | 70% |
| $M = 2, P = 3$ | 20% | 30% | 40% | 70% |

There are actually other performance criteria where joint space-time processing in 1D-ST STAR readily outperforms sequential space and time processing in 2D RAKE-type receivers. In terms of complexity, joint space-time processing requires less computations than sequential space and time processing. As shown in Table 10.2, reduction in the number of operations with joint

processing is significant with $M = 4$ antennas and increases with $M = 2$ antennas. The computational gain shrinks, however, with larger antenna-arrays.

In terms of robustness to changes in propagation conditions, 1D-ST STAR is insensitive to multipath power profile variations. Indeed, it requires optimization of a single step-size value $\mu$ regardless of the average multipath power fractions. On the other hand, 2D STAR requires optimization of multiple step-sizes $\mu_p$ with constant adjustments to the average multipath power fractions[20], in order to cope with changing propagation conditions. Without such adjustments, simulations with variable multipath power profiles (not shown for lack of space) suggest that 2D STAR looses about 0.5 dB in SNR (with steps-size values optimized for equal-power paths) while 1D-ST STAR performs the same. Joint space-time processing in 1D-ST STAR is hence more robust to changes in propagation conditions than sequential space and time processing in current 2D RAKE-type receivers and alleviates the demanding burden of continuous step-size optimization.

So far the comparisons between 1D-ST and 2D-STAR have been limited to the link level. In fact, 1D-ST STAR has additional benefits at the system level where reduced variance of the total received power reduces the probability of outage [25]. Indeed, more accurate channel estimation with 1D-ST DFI results in more accurate estimation of the total received power. Additionally, while the power variations of the feedback signal $\hat{s}_n$ of 1D-ST DFI in (10.39) are "equalized" by power control, those of the feedback signal $\hat{s}_{p,n}$ of 2D DFI in (10.15) are not. Reduced variation in the power of the feedback signal further reduces channel estimation and power control errors and hence increases the performance advantage of 1D-STAR over 2D STAR at the system level. This is however beyond the scope of this contribution.

In summary, joint space-time processing in 1D-ST STAR outperforms sequential space and time processing in current 2D RAKE-type receivers in many ways[21]:

- it requires less complexity, especially with small antenna arrays;
- it increases robustness to changing propagation conditions and alleviates the demanding burden of continuous steps-size optimization;
- it identifies multipath Rayleigh channels faster and more accurately and offers noticeable[22] link-level SNR gains at very high Doppler;
- it reduces power control errors and offers potential system-level capacity gains (see footnote 22).

[20] If required, notice that (10.52) enables instantaneous optimization of variable step-sizes $\mu_{p,n}$ using $\varepsilon^2_{p,n}$ instead of $\bar{\varepsilon}^2_{p,n}$.

[21] Another advantage of joint processing is that it increases the dimension of the observation space from $M$ (or $P$) to $MP$ thereby allowing implementation of null constraints with less noise enhancement and more efficient interference suppression [7]. This is however beyond the scope of this contribution.

[22] In fact, performance evaluations at the link and system levels with active synchronization [5] both showed significant gains of blind 2D STAR over the blind 2D RAKE, more so at high Doppler.

We previously reported on the capacity gains achievable by 1D-ST STAR over 2D STAR and 2D RAKE-type receivers with orthogonal Walsh-modulated CDMA signals [20]. There we proposed similar incremental upgrades of the 2D DFI procedure in 2D STAR (see Sect. 10.4) that ultimately implement *blind coherent*[23] ST-MRC with 1D-ST STAR. With $\mathcal{M}$PSK modulations so far, we have been able to implement *blind quasi-coherent* (*i.e.*, within constellation-invariant rotation point) ST-MRC. In the next section we propose further upgrades of 1D-ST STAR that implement *quasi-blind* (*i.e.*, with very weak pilot signals) or *"asymptotically" blind coherent* ST-MRC.

## 10.6 The Pilot-Assisted 1D-ST STAR

Blind 1D-ST STAR implements *quasi-coherent* ST-MRC by identifying the channel within a constellation-invariant phase rotation. Conventional use of pilot signals [12]-[16] in RAKE-type receivers allows channel identification[24] without phase ambiguity and hence enables implementation of *reference-assisted coherent* ST-MRC. It requires however large-enough pilot-power or -overhead fractions to guarantee accurate channel identification. We propose instead enhanced use of pilot signals with much weaker power or overhead to resolve then compensate the constellation-invariant phase rotation of the channel identified blindly and more accurately. We hence implement *quasi-blind* (*i.e.*, with very weak pilot signals) or *"asymptotically" blind coherent* ST-MRC. Enhanced channel identification and reduction of the pilot power or overhead combined result in a total SNR gain of 1 dB and enable significant battery power-savings and spectrum-efficiency gains.

### 10.6.1 Data Model with Pilot Signals

So far we differentially encoded the data symbols $\underline{b}_n$ as $b_n$ in (10.2) to compensate for the phase ambiguity inherent to blind channel identification by differential decoding with hard DFI (or demodulation with soft DFI, see Sect. 10.5.3). Here we exploit pilot signals to either avoid or resolve this ambiguity. Hence we avoid differential encoding and simply assign $b_n = \underline{b}_n$ in the following. In both blind and pilot-assisted processing we spread the data symbols $b_n$ by a data code and hence mark the corresponding data-channel parameters with superscript $\delta$. In pilot-assisted processing, we may

[23] With orthogonal Walsh modulation, the constellation set is $\mathcal{C}_{\mathcal{M}} = \{0, 1\}$ after despreading and the only constellation-invariant phase rotation possible is $2\pi$ (*i.e.*, $\mathcal{R}_{\mathcal{M}} = \{1\}$), hence no ambiguity is possible with hard DFI (see Sect. 10.4.5).

[24] Note that these techniques (*i.e.*, [12]-[16]) estimate each diversity finger with a multiple-tap low-pass filter. With less computations here, we identify each finger with an optimized single-tap adaptive-filter using the DFI procedure (see Sects. 10.6.2 and 10.6.4).

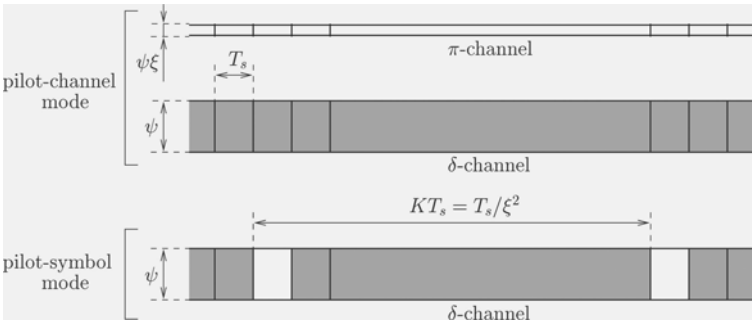


**Fig. 10.12.** Pilot modes (data signals are in grey and pilot signals are in white).

**Table 10.3** Description of the tested versions of 1D-ST STAR.

| | pilot mode | pilot use |
|---|---|---|
| Rx1 | none | none (*i.e.*, blind without pilot) |
| Rx2 | pilot-channel | channel identification (*i.e.*, conventional) |
| Rx3 | pilot-channel | ambiguity resolution (*i.e.*, enhanced) |
| Rx4 | pilot-symbol | channel identification (*i.e.*, conventional) |
| Rx5 | pilot-symbol | ambiguity resolution (*i.e.*, enhanced) |

either code-multiplex the spread data with a pilot or simply insert (*i.e.*, time-multiplex) pilot symbols in the data channel (see Fig. 10.12) and hence mark the corresponding pilot-channel parameters or pilot symbols with superscript $\pi$, respectively. Hence we simply rewrite the data observation vector of (10.37) as follows:

$$\underline{Z}_n^{\delta} = \underline{H}_n s_n^{\delta} + \underline{N}_n^{\delta} = \underline{H}_n \psi_n b_n + \underline{N}_n^{\delta}. \tag{10.57}$$

Similarly when a pilot-channel is used (see Fig. 10.12), we form the $MP \times 1$ pilot observation vector as:

$$\underline{Z}_n^{\pi} = \underline{H}_n s_n^{\pi} + \underline{N}_n^{\pi} = \underline{H}_n \xi \psi_n + \underline{N}_n^{\pi}, \tag{10.58}$$

where $\xi^2 < 1$ denotes the allocated pilot-to-data power ratio and $\underline{N}_n^{\pi}$ is a zero-mean space-time uncorrelated Gaussian noise vector with the same covariance matrix as $\underline{N}_n^{\delta}$ (*i.e.*, $\mathbf{R}_{\underline{N}} = \sigma_N^2 \mathbf{I}_{MP}$). When a pilot-symbol is used (see Fig. 10.12), the data sequence $b_n$ is simply assigned a constant "1" once every $K$ symbols, although insertion of pilot blocks is possible. Hence we have $b_{n'K} = 1$ and $s_{n'K}^{\pi} = s_{n'K}^{\delta} = \psi_{n'K}$. In this case, $\xi^2 = 1/K$ denotes the allocated pilot-to-data overhead ratio.

In the following, we investigate the five versions of STAR summarized in Table 10.3, the first reference version Rx1 being the blind 1D-ST STAR with hard DFI already described in Sect. 10.5.3.

### 10.6.2 1D-ST STAR with Conventional Pilot-Channel Use

The second version of STAR, denoted by Rx2 (see Table 10.3), uses a pilot-channel for conventional channel identification [14], [16] (see footnote 24). It exploits the fact that the pilot signal is a known reference signal (*a priori* constant "1") to feed it back to the 1D-ST DFI procedure of (10.39) modified[25] as follows [18]:

$$\underline{\hat{H}}_{n+1} = \underline{\hat{H}}_n + \mu \left( \underline{Z}_n^{\pi} - \underline{\hat{H}}_n \hat{s}_n^{\pi} \right) \hat{s}_n^{\pi}, \tag{10.59}$$

where $\hat{s}_n^{\pi} = \xi \hat{\psi}_n$ denotes the feedback signal with known positive sign. Estimation of the total received power $\hat{\psi}_n^2$ and the tentative symbol estimate $\hat{b}_n$ follow by (10.35) and (10.32).

Note that the modified DFI procedure above operates on the pilot despread vector $\underline{Z}_n^{\pi}$ with a constellation set $\mathcal{C}_1 = \{1\}$ (*i.e.*, pilot symbol is constant "1") and a rotation set $\mathcal{R}_1 = \{1\}$ (*i.e.*, no possible ambiguity). As a result, it identifies the channel without ambiguity (*i.e.*, $a_n = 1$) and hence estimates the data symbol and the decision variable as follows:

$$\underline{\hat{b}}_n = \hat{b}_n, \tag{10.60}$$

$$d_n = \tilde{s}_n^{\delta}, \tag{10.61}$$

where $\tilde{s}_n^{\delta}$ in (10.41) denotes now the soft output of coherent ST-MRC. In contrast to Rx1, Rx2 no longer requires differential decoding of (10.36) and differential demodulation of (10.29) in the detection steps above. Hence it reduces detection errors over both channel-uncoded and coded transmissions by implementing "fully" coherent instead of quasi-coherent ST-MRC.

Note however that Rx2 identifies the channel using the pilot feedback signal $\hat{s}_n^{\pi}$ with power $\xi^2 \bar{\psi}^2 < \bar{\psi}^2$. Analytical results of Sect. 10.5.4 apply to Rx2 and hence yield the following optimum step-size and minimum misadjustment as well as the corresponding time constant:

$$\mu_{Rx2,\text{opt}} = 2 \left[ (\pi f_D T_s) \,/\, \left( \sqrt{P} \xi^2 \bar{\psi}^2 \sigma_N \right) \right]^{\frac{2}{3}}, \tag{10.62}$$

$$\beta_{Rx2,\text{min}}^2 = \frac{3}{2} \left[ (\pi f_D T_s) \,/\, \left( \sqrt{P} \xi^2 SNR_{\text{in}} \right) \right]^{\frac{2}{3}}, \tag{10.63}$$

$$\tau_{Rx2,\text{opt}} \simeq \frac{1}{4} \left[ \sqrt{P} / \left( \pi f_D T_s \xi \sqrt{SNR_{\text{in}}} \right) \right]^{\frac{2}{3}}. \tag{10.64}$$

Expressions above indicate that Rx2 performs worse than Rx1 in channel identification in terms of both misadjustment and convergence speed. Despite increased detection errors due to differential decoding, Rx1 may outperform Rx2 from reduced channel identification errors as shown later by simulations.

[25] Note that the DFI step of (10.59) could be updated at a slower rate if the pilot signal is transmitted in short bursts on the pilot channel. Extension in this case is *ad hoc*.

### 10.6.3 1D-ST STAR with Enhanced Pilot-Channel Use

The third version of STAR, denoted by Rx3 (see Table 10.3), is a hybrid of Rx1 and Rx2. Like Rx1, it applies the blind DFI procedure of (10.39) and (10.44) to estimate the channel within a constellation-invariant phase ambiguity $a_n$. Like Rx2, its uses a pilot-channel. However, with much weaker power it exploits the pilot more efficiently to accurately estimate then resolve the phase ambiguity $a_n \simeq r_k \in \mathcal{R}_{\mathcal{M}}$ [18]. Noticing that the pilot signal component estimate[26] given by:

$$\tilde{s}_n^{\pi} = \underline{\hat{H}}_n^H \underline{Z}_n^{\pi}/M \simeq a_n \psi_n \xi + \eta_n^{\pi}, \tag{10.65}$$

is based on a noisy value of $a_n$, Rx3 estimates it by hard decision over the soft output $\hat{s}_n^{\pi}$ averaged over consecutive blocks of $A$ samples, giving for $n \in \{n'A, \ldots, (n'+1)A-1\}$ [18]:

$$\tilde{a}_n = \tilde{a}_{n'} = \frac{\sum_{i=0}^{A-1} \tilde{s}_{n'A+i}^{\pi}}{A}, \tag{10.66}$$

$$\hat{a}_n = \hat{a}_{n'} = \simeq r_k = \arg\min_{r_k \in \mathcal{R}_{\mathcal{M}}} \{|\tilde{a}_n - r_k|\}. \tag{10.67}$$

The averaging step[27] above enables accurate estimation of $a_n$ with a much weaker pilot power [18]. Hence, Rx3 estimates the data symbol and the decision variable by simple phase ambiguity compensation as follows [18]:

$$\underline{\hat{b}}_n = \hat{a}_n^* \hat{b}_n, \tag{10.68}$$

$$d_n = \hat{a}_n^* \tilde{s}_n^{\delta}, \tag{10.69}$$

and thereby implements coherent ST-MRC, like Rx2, with the same benefits in reducing symbol detection errors over Rx1.

Note however that expressions for $\mu_{Rx3,\text{opt}}$, $\beta^2_{Rx3,\min}$ and $\tau_{Rx3,\text{opt}}$ are exactly those of Rx1 in (10.48) to (10.50), respectively. Rx3 therefore combines both advantages of Rx1 and Rx2 by 1) exploiting a much weaker pilot than Rx2 to resolve the phase ambiguity and implement coherent detection and 2) by exploiting the data channel with much more power than the pilot channel for more accurate channel identification. Simulations will later confirm the performance advantage of Rx3 over both Rx1 and Rx2.

[26] The power fraction in $\tilde{s}_n^{\pi}$ can be exploited in enhancing power estimation in (10.35) [18].

[27] Long-term averaging is made possible by the "anchoring" mechanism of hard DFI (see Sect. 10.4.5). With soft DFI, the ambiguity rotates continuously (see Fig. 10.3) and prevents accurate estimation of $a_n$ by long-term averaging.

### 10.6.4 1D-ST STAR with Conventional Pilot-Symbol Use

The fourth version of STAR, denoted by Rx4 (see Table 10.3), uses pilot symbols for conventional channel identification [12], [13], [15], [16] (see footnote 24). Its DFI procedure is similar to that of Rx1 in (10.39). However, it only feeds back the signal components containing the pilot symbols inserted in the data sequence once every $K$ symbols [19]:

$$\underline{\hat{H}}_{(n'+1)K} = \underline{\hat{H}}_{n'K} + \mu \left( \underline{Z}^{\delta}_{n'K} - \underline{\hat{H}}_{n'K} \hat{s}^{\pi}_{n'K} \right) \hat{s}^{\pi}_{n'K}, \tag{10.70}$$

where $\hat{s}^{\pi}_{n'K} = \hat{\psi}_{n'K}$. Note that the modified DFI procedure above operates at time corresponding to the pilot-symbol indices $n'K$ on the data despread vector $\underline{Z}^{\delta}_{n'K}$ with a constellation set $\mathcal{C}_1 = \{1\}$ (*i.e.*, pilot symbol is constant "1") and a rotation set $\mathcal{R}_1 = \{1\}$ (*i.e.*, no possible ambiguity). Similarly to Rx2, the DFI procedure of Rx4 identifies the channel without ambiguity (*i.e.*, $a_n = 1$) and allows estimation of $\underline{\hat{b}}_n$ and $d_n$ using (10.60) and (10.61), respectively.

Notice, however, that Rx4 updates the DFI procedure less frequently than Rx2, namely at the pilot-symbol rate $1/KT_s$. Exploiting again the analytical results of Sect. 10.5.4, we have:

$$\mu_{Rx4,\mathrm{opt}} = 2 \left[ (\pi f_D K T_s) \,/\, \left( \sqrt{P} \bar{\psi}^2 \sigma_N \right) \right]^{\frac{2}{3}} = \mu_{Rx2,\mathrm{opt}}, \tag{10.71}$$

$$\beta^2_{Rx4,\min} = \frac{3}{2} \left[ (\pi f_D K T_s) \,/\, \left( \sqrt{P} \xi^2 SNR_{\mathrm{in}} \right) \right]^{\frac{2}{3}} = \beta^2_{Rx2,\min}, \tag{10.72}$$

$$\tau_{Rx4,\mathrm{opt}} \simeq \frac{K}{4} \left[ \sqrt{P} / \left( \pi f_D K T_s \sqrt{SNR_{\mathrm{in}}} \right) \right]^{\frac{2}{3}} = \tau_{Rx2,\mathrm{opt}}, \tag{10.73}$$

and hence find that Rx2 and Rx4 identify the channel equally well when they use the same pilot power and overhead fractions[28] (*i.e.*, $K = 1/\xi^2$) [19].

On the one hand, the channel subsampled at the DFI-update instants appears to vary $K$ times faster with a relative normalized Doppler $Kf_DT_s$. Thus channel identification errors can be expected to increase with faster time-variations. On the other hand, the power of the feedback signal in Rx4, $|\hat{s}^{\pi}_{n'K}|^2 = \hat{\psi}^2_{n'K}$, is $K$ times stronger than in Rx2 where $|\hat{s}^{\pi}_n|^2 = \xi^2 \hat{\psi}^2_n = \hat{\psi}^2_n / K$. This suggests that channel identification errors will decrease with stronger feedback signals. Analysis of Sect. 10.5.4 shows a non-trivial result that the corresponding loss and gain in the performance of adaptive channel identification cancel each other [19]. The minimum channel misadjustment achievable remains constant if we increase or decrease both the relative Doppler and the feedback-signal's power by the same factor $K$. Later we confirm by simulations that Rx2 and Rx4 perform equally well.

[28] A similar conclusion regarding misadjustment was reached in [16] based on channel estimation with low-pass filtering (see footnote 24).

### 10.6.5 1D-ST STAR with Enhanced Pilot-Symbol Use

Similarly to Rx3, the fifth version of STAR denoted by Rx5 (see Table 10.3) is a hybrid of Rx1 and Rx4. It applies the blind DFI procedure of (10.39) and (10.44) to estimate the channel within a constellation-invariant phase ambiguity $a_n$. However, it uses the pilot symbols to estimate then resolve the phase ambiguity $a_n$ [19]. Assume for simplicity that a block of $A$ consecutive symbols contains exactly $Q$ pilot symbols (*i.e.*, $A = QK$). Rx4 modifies (10.66) simply by averaging the pilot signal component estimate over these $Q$ symbols for $n \in \{n'A, \ldots, (n'+1)A-1\}$ [18]:

$$\tilde{a}_n = \frac{\sum_{i=0}^{Q-1} \hat{s}^{\pi}_{n'A+Ki}}{Q}, \tag{10.74}$$

before estimating $a_n$ by hard decision in (10.67). Similarly to Rx3, Rx5 thereby resolves the phase ambiguity and hence estimates $\underline{\hat{b}}_n$ and $d_n$ using (10.69) and (10.68), respectively. Like Rx3, expressions for $\mu_{Rx5,\text{opt}}$, $\beta^2_{Rx5,\min}$ and $\tau_{Rx5,\text{opt}}$ are exactly those of Rx1 in (10.48) to (10.50), respectively.

Notice that Rx5 in (10.74) estimates the pilot-signal component from $K = A/Q$ fewer values than Rx3 in (10.66). The variance of the residual noise present in $\tilde{a}_n$ is thereby increased by factor $K$. However, bear in mind that the pilot-signal power in Rx5 is $K$ times stronger than in Rx3. Indeed, in contrast to (10.65) we have:

$$\tilde{s}^{\pi}_n = \underline{\hat{H}}^H_n \underline{Z}^{\pi}_n / M \simeq a_n \psi_n + \eta^{\pi}_n. \tag{10.75}$$

The SNR of $\tilde{a}_n$ before phase ambiguity estimation in (10.67) is therefore the same for both receiver versions. Despite the differences between Rx3 and Rx5, the averaging step in (10.66) or (10.74) results in the same phase estimation error. In the following section we confirm that Rx3 and Rx5 have equivalent performance.

### 10.6.6 Performance Gains with Enhanced Pilot Use

In Fig. 10.13, we compare the SER performance of the various receiver versions of 1D-ST STAR described previously (see Table 10.12) for BPSK, QPSK, 8PSK and 16QAM[29]. In Sect. 10.4.5, we have shown that the anchoring mechanism of hard DFI works well with $\mathcal{M}$QAM modulations (see Fig. 10.8). Hence its useful feature of casting the phase ambiguity in the rotation set $\mathcal{R}_{\mathcal{M}}$ can be efficiently exploited to estimate and then compensate the phase ambiguity with enhanced use of pilot signals in 16QAM-modulated Rx3 and Rx5.

[29] Note that the blind version Rx1, inapplicable with $\mathcal{M}$QAM modulations, is not evaluated in Fig. 10.13(d).

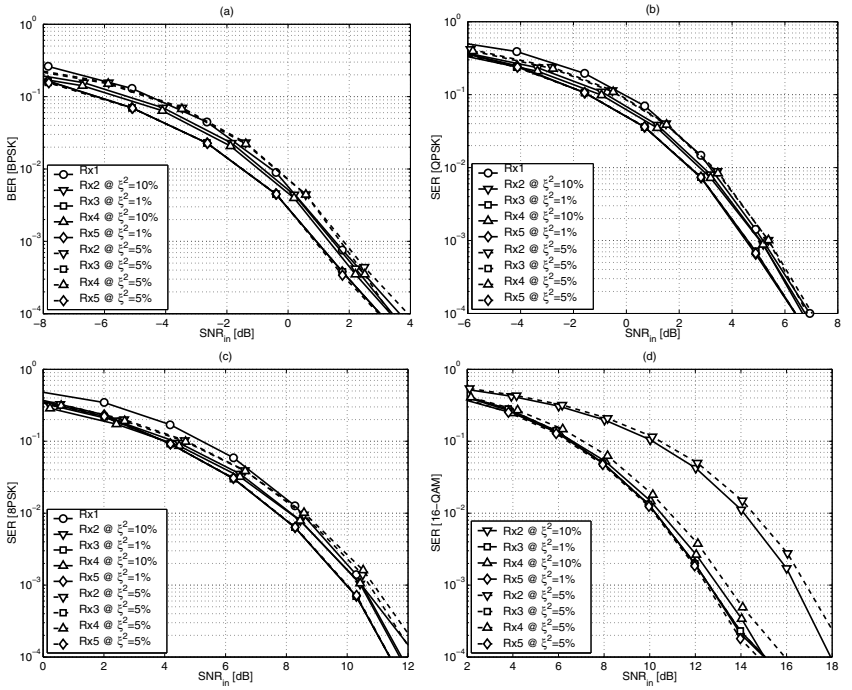


**Fig. 10.13.** SER vs. SNR in dB for different versions of 1D-ST STAR (see Table 10.12) with optimum step-size values. (a): BPSK, (b): QPSK, (c): 8PSK, (d): 16QAM.

Simulation results shown in Fig. 10.13 indicate that more efficient exploitation of pilot channels or symbols for only phase-ambiguity resolution outperforms their conventional use for channel-identification regardless of the modulation employed. They also suggest that pilot-channel and pilot-symbol versions, with either conventional or enhanced pilot use, perform similarly for all modulations except 16QAM with conventional pilot, thereby confirming our analytical assertions[30].

Note that the receiver versions with enhanced pilot use (*i.e.*, Rx3 and Rx5) perform practically the same with 1 or 5% fractions of the pilot power or overhead. This result shows that long-term averaging in (10.66) and (10.74) indeed significantly reduces phase ambiguity estimation errors in (10.67) from very weak pilot signals (we used $A = 500$ in all simulations of Fig. 10.13). On the other hand, the receiver versions with conventional pilot use (*i.e.*, Rx2 and Rx4) see their performance drop when the pilot power or overhead

[30] The theoretical results of Sect. 10.5.4 derive from a convergence and performance analysis in [17] that assumes a constant-modulus modulation. Conventional identification with weak power or overhead fractions increases channel estimation errors and likely contributes to further increasing the mismatch with analysis.

fraction is reduced by half from 10 to 5%. Simulations actually indicate that Rx2 and Rx4 with 10% fraction perform worse than Rx3 and Rx5 with 1% fraction only. They also suggest that Rx2 and Rx4 perform even worse than blind Rx1 at higher SNR, more so with reduced power fractions.

Figure 10.13 actually suggests that Rx3 and Rx5 with 1% power or overhead fraction offer about 0.8 dB gain in SNR over Rx2 and Rx4 with 5% fraction, and about 0.5 dB over Rx2 and Rx4 with 10%. However, capacity gains achievable at the system level by the reduction of the pilot-signals' interference from 5 and 10% to 1% account for "equivalent" SNR gains of roughly 0.2 (*i.e.*, $10\log_{10}(1.05/1.01)$) and 0.4 dB (*i.e.*, $10\log_{10}(1.1/1.01)$) at the link level, respectively. The total performance gain of Rx3 and Rx5 over Rx2 and Rx4 with either power/overhead fraction is hence in the range of 1 dB. Reduced power variations and power control errors due to blind identification of the data channel with stronger signals (see Sect. 10.5.4) should further increase the performance advantage of Rx3 and Rx5 over Rx2 and Rx4 at the system level.

The discussion above suggests that optimization of the step-size alone does not allow for fair comparisons without simultaneous optimization of the pilot power or overhead fraction $\xi^2 = 1/K$, in order to reflect additional gains at the system level due to enhanced pilot use with significantly reduced pilot power or overhead [18], [19]. This is beyond the scope of this contribution. In [18], [19] however, we provide analytical means for optimizing the five receiver versions of 1D-ST STAR at the system level and show that enhanced pilot use allows for significant spectrum efficiency gains in most practical situations.

Overall, pilot-assisted space-time receivers with conventional pilot use require pilot-power or -overhead fractions large enough to guarantee accurate channel identification and reliable data detection at the receiver. Pilot-assisted space-time receivers with enhanced pilot use require much weaker power or overhead (*i.e.*, in the range of 1%) to resolve then compensate the constellation-invariant phase rotation of the channel identified blindly and more accurately. They hence implement *quasi-blind* or *"asymptotically" blind* (*i.e.*, with very weak pilot signals) *coherent* ST-MRC. Enhanced channel identification and reduction of the pilot power or overhead combined result in a total SNR gain of 1 dB and enable significant battery power-savings and spectrum-efficiency gains [18], [19]. Similar gains can be achieved on the downlink [21].

## 10.7 Conclusions

Several improvements are proposed to the 2D-RAKE, a widely used space-time adaptive receiver which combines CDMA signals sequentially, first in space, then in time. Ultimately we arrive at a more efficient one-dimensional joint space-time (1D-ST) adaptive processor, STAR, the spatio-temporal array-receiver. Advantages of STAR are twofold.

First, STAR carries out an improved combining operation that approaches that of blind coherent space-time MRC. In the blind mode (*i.e.*, without a pilot), the 2D RAKE sequentially implements noncoherent spatial MRC then temporal EGC while STAR implements quasi-coherent (*i.e.*, within a constellation-invariant phase ambiguity) joint ST-MRC. By improving the combing rule STAR outperforms the 2D RAKE by about 2 dB gain in SNR. In the pilot-assisted mode, the 2D RAKE uses the pilot for conventional identification and hence requires a strong pilot to accurately implement reference-assisted coherent space and time MRC sequentially. On the other hand, STAR requires a much weaker pilot to estimate then compensate the constellation-invariant phase ambiguity of the channel identified blindly and more accurately, and hence implements quasi-blind or asymptotically blind coherent joint ST-MRC. Enhanced channel identification and reduction of the pilot power or overhead (in the range of 1%) combined result in a total SNR gain of 1 dB and enable significant battery power-savings and spectrum-efficiency gains.

Second, STAR outperforms the 2D RAKE in many ways by implementing joint space-time processing in a 1D-ST structured adaptive receiver. Indeed, we provide novel and non-trivial analytical results that clearly establish the performance advantage of one-dimensional joint space-time processing in 1D-ST STAR over two-dimensional spatial then temporal sequential processing in the 2D RAKE-type adaptive receivers widely used today. We show that 1D-ST structured adaptive receivers reduce both complexity and channel identification errors, increase robustness to changing propagation conditions, and speed up convergence over multipath Rayleigh-fading channels. These gains, validated by simulations, translate immediately into enhanced receiver performance.

## References

1. 3rd Generation Partnership Project (3GPP), Technical Specification Group (TSG), Radio Access Network (RAN), Working Group (WG4), *UE Radio Transmission and Reception (FDD)*, TS 25.101, V3.4.1, 2000.
2. 3rd Generation Partnership Project (3GPP), Technical Specification Group (TSG), Radio Access Network (RAN), Working Group (WG4), *Base Station Conformance Testing (FDD)*, TS 25.141, V3.3.0, 2000.
3. 3rd Generation Partnership Project, Technical Specification Group (TSG), Radio Access Networks (RAN), *Physical Layer Aspects of UTRA High Speed Downlink Packet Access*, 3GPP TR 25.848, V4.0.0, 2001.
4. S. Affes and P. Mermelstein, "A new receiver structure for asynchronous CDMA: STAR - The spatio-temporal array-receiver," *IEEE J. Selec. Areas Comm.*, vol. 16, no. 8, pp. 1411–1422, Oct. 1998.
5. K. Cheikhrouhou, S. Affes, and P. Mermelstein, "Impact of synchronization on performance of enhanced array-receivers in wideband CDMA networks," *IEEE J. Selec. Areas Comm.*, vol. 19, no. 12, pp. 2462–2476, Dec. 2001.

6. H. Hansen, S. Affes, and P. Mermelstein, "A beamformer for CDMA with enhanced near-far resistance," in *Proc. IEEE ICC*, 1999, vol. 3, pp. 249–253.
7. S. Affes, H. Hansen, and P. Mermelstein, "Interference subspace rejection: a framework for multiuser detection in wideband CDMA," *IEEE J. Selec. Areas Comm.*, vol. 20, no. 2, pp. 287–302, Feb. 2002.
8. B. Suard, A. F. Naguib, G. Xu, and A. Paulraj, "Performance of CDMA mobile communication systems using antenna arrays," in *Proc. ICASSP*, vol. IV, 1993, pp. 153–156.
9. B. H. Khalaj, A. Paulraj, and T. Kailath, "2D RAKE receivers for CDMA cellular systems," in *Proc. GLOBECOM*, 1994, pp. 400–404.
10. A. F. Naguib and A. Paulraj, "Effects of multipath and base-station antenna arrays on uplink capacity of cellular CDMA," in *Proc. GLOBECOM*, 1994, pp. 395–399.
11. A. F. Naguib, *Adaptive Antennas for CDMA Wireless Networks*, Ph.D. Dissertation, Stanford University, USA, 1996.
12. J. K. Cavers, "An analysis of pilot symbol assisted modulation for Rayleigh fading channels," *IEEE Trans. Vehic. Tech.*, vol. 40, no. 4, pp. 686–693, Nov. 1991.
13. C. D'Armours, M. Moher, and A. Yongaḡlu, "Comparison of pilot-symbol assisted and differentially detected BPSK for DS-CDMA systems employing RAKE receivers in Rayleigh fading channels," *IEEE Trans. Vehic. Tech.*, vol. 47, no. 4, pp. 1258–1267, Nov. 1997.
14. P. Schramm, "Analysis and optimization of pilot-channel-assisted BPSK for DS-CDMA systems," *IEEE Trans. Comm.*, vol. 46, no. 9, pp. 1122–1124, Sept. 1998.
15. P. Schramm, "Pilot symbol assisted BPSK on Rayleigh fading channels with diversity: performance analysis and parameter optimization," *IEEE Trans. Comm.*, vol. 46, no. 12, pp. 1560–1563, Dec. 1998.
16. F. Ling, "Optimal reception, performance bound, and cutoff rate analysis of reference-assisted coherent CDMA communications with applications," *IEEE Trans. Comm.*, vol. 47, no. 10, pp.1583–1592, Oct. 1999.
17. S. Affes and P. Mermelstein, "Comparison of pilot-assisted and blind CDMA array-receivers adaptive to Rayleigh fading rates," in *Proc. of IEEE PIMRC*, 1999, vol. 3, pp. 1186–1192.
18. S. Affes, A. Louzi, N. Kandil, and P. Mermelstein, "A high capacity CDMA array-receiver requiring reduced pilot power," in *Proc. of IEEE GLOBECOM*, 2000, vol. 2, pp. 910–916.
19. S. Affes, N. Kandil, and P. Mermelstein, "Efficient use of pilot signals in wideband CDMA array-receivers," submitted for publication, 2002.
20. S. Affes and P. Mermelstein, "A blind coherent spatio-temporal processor of orthogonal Walsh-modulated CDMA signals," *Wiley Journal on Wireless Communications and Mobile Computing*, accepted for publication, to appear in 2002.
21. S. Affes, A. Saadi, and P. Mermelstein, "Pilot-assisted STAR for increased capacity and coverage on the downlink of wideband CDMA networks," in *Proc. of IEEE SPAWC*, 2001, pp. 310–313.
22. N. A. B. Svensson, "On differentially encoded star 16QAM with differential detection and diversity," *IEEE Trans. Vehic. Tech.*, vol. 44, no. 3, pp. 586–593, Aug. 1995.

23. J. G. Proakis, *Digital Communications*, McGraw Hill, 3rd Edition, 1995.
24. M. K. Simon and M.-S. Alouini, "A unified approach to the probability of error of noncoherent and differentially coherent modulations over generalized fading channels," *IEEE Trans. Comm.*, vol. 46, no. 12, pp. 1625–1638, December 1998.
25. A. Jalali and P. Mermelstein, "Effects of diversity, power control, and bandwidth on the capacity of microcellular CDMA systems," *IEEE J. Selec. Areas Comm.*, vol. 12, no. 5, pp. 952–961, June 1994.